The Neoproterozoic Visingsö Group of southern Sweden: Lithology, sequence stratigraphy and provenance of the Middle Formation

Viktor Ahrenstedt

Dissertations in Geology at Lund University,
Master's thesis, no 551
(45 hp/ECTS credits)

Department of Geology
Lund University
2018

The Neoproterozoic Visingsö Group of southern Sweden: Lithology, sequence stratigraphy and provenance of the Middle Formation

Master's thesis

Viktor Ahrenstedt

Department of Geology
Lund University
2018

Contents

Cover Picture: Outcrop of the Visingsö Group from the Näs locality, Visingsö, Sweden. Photo: Ahrenstedt.

The Neoproterozoic Visingsö Group of southern Sweden: Lithology, sequence stratigraphy and provenance of the Middle Formation

VIKTOR AHRENSTEDT

Ahrenstedt, V., 2018: The Neoproterozoic Visingsö Group of southern Sweden: Lithology, sequence stratigraphy and provenance of the Middle Formation. *Dissertations in Geology at Lund University*, No. 551, 46 pp. 45 hp (45 ECTS credits).

Abstract: The depositional setting of the Neoproterozoic Visingsö Group has long been a subject of discussion. This study aims to provide additional insights into the lithological composition and provenance of the sediments and to provide a sequence stratigraphic framework in order to define the depositional setting. It focuses on rocks belonging to the Middle Formation of the Visingsö Group located at the Näs locality, Visingsö, Sweden. The methods employed included descriptions of lithology, stratigraphic variations and identification of sedimentary patterns through detailed facies logs. Furthermore LA-ICP-MS analyses of U/Pb ages on detrital zircons were performed to determine their provenance. The sediments are characterized by an immature composition, short transport distance and wave-dominated deposition. The sedimentary cycles are composed of coarsening-upwards intervals terminated by short transgressive episodes. Identified detrital ages of zircons are largely composed of ages that can be found in the region. The sequence stratigraphic framework is in accord with existing rift-basin models and showed that deposition was controlled by tectonic activity that created the space necessary for the deposition of sediments. This newly created space was filled in large parts by locally derived material with a smaller, more far-travelled, component.

Keywords: Neoproterozoic, Visingsö Group, sequence stratigraphy, provenance, lithology.

Supervisor(s): Mikael Calner

Subject: Sedimentary Geology, Geochronology

Viktor Ahrenstedt, Department of Geology, Lund University, Sölvegatan 12, SE-223 62 Lund, Sweden. E-mail: viktor.ahrenstedt@gmail.com

Den sydsvenska neoproterozoiska Visingsögruppen: Litologi, sekvensstratigrafi och provenans av den Mellersta formationen

VIKTOR AHRENSTEDT

Ahrenstedt, V., 2018: Den sydsvenska neoproterozoiska Visingsögruppen: Litologi, sekvensstratigrafi och provenans av den Mellersta formationen. *Examensarbeten i geologi vid Lunds universitet*, Nr. 551, 46 sid. 45 hp.

Sammanfattning: Det har länge pågått diskussioner om hur Visingsögruppen blev avsatt. Målet med den här studien är att få mer insikt i sedimentens litologiska sammansättning, provenans och genom att sätta upp ett sekvensstratigrafiskt ramverk kunna definiera depositionsprocesser. Studien fokuserade på sediment som tillhör den Mellersta formationen i Visingsögruppen, belägna vid Näs, Visingsö, Sverige. Metoderna som används inkluderar beskrivningar av litologi, stratigrafiska variationer och identifiering av sedimentära mönster genom detaljerade loggar. Vidare så användes LA-ICP-MS analyser för U/Pb dateringar av detritala zirkoner för att bestämma deras provenans. Sedimenten defineras av en omogen sammansättning, korta transportsträckor och vågdominerad avsättning. De sedimentära cyklerna är sammansatta av intervall med kontinuerligt ökande kornstorlek som avslutas med transgressiva episoder. De detritala zirkonernas åldrar stämmer i hög grad med åldrar som kan hittas regionalt. Det sekvensstratigrafiska ramverket överensstämmer med existerande modeller för riftbassänger och visar att avsättningen är kontrollerad av tektonik som skapar det nödvändiga utrymmet för att deposition ska kunna ske. Detta nyskapade utrymme fylldes igen av lokalt material och en mindre komponent av längre transporterat material.

Nyckelord: Neoproterozoikum, Visingsögruppen, sekvensstratigrafi, provenans, litologi.

Handledare: Mikael Calner

Ämnesinriktning: Sedimentär geologi, geokronologi

Viktor Ahrenstedt, Geologiska institutionen, Lunds Universitet, Sölvegatan 12, 223 62 Lund, Sverige. E-post: viktor.ahrenstedt@gmail.com

1 Introduction

The Neoproterozoic Visingsö Group has been studied for well over 100 years. Owing to poor exposure of the successions, tectonic influence and lithological homogeneity few studies have touched on its depositional history. This paper aims to summarise previous work and provide additional insights into how these sedimentary rocks were formed. It focuses on the outcrops at Näs that exhibits the Middle Formation of the Visingsö Group and is located on the island of Visingsö in Lake Vättern, south central Sweden.

This project aimed to produce centimetre scale facies logs with detailed descriptions of the lithology and stratigraphic variations of the outcrops at the Näs locality. Sedimentary cycles and patterns were identified in order to define individual sequences. A sequence stratigraphical framework could then be produced in conjunction with existing sequence stratigraphical models. These results were used to determine the depositional processes involved in the formation of the rocks.

Furthermore the project aimed to provide insights into the provenance of the sediments through radiometric dating using LA-ICP-MS analyses of detrital zircons and comparisons of these ages to known ages of potential source rocks.

2 Background

2.1 Previous work

The Visingsö Group is named after the Island of Visingsö situated in the south-central parts of Lake Vättern (Nathorst 1879a). The first time that the Visingsö Group was referred to as an independent sedimentary succession was, according to Zenzén (1925), in a travel-diary by J.A. Gyllenhaal in 1775 who distinguished the Visingsö Group from the nearby Cambro-Silurian sediments of the province of Östergötland.

The Visingsö Group was discussed intensely in the late 1800's (e.g. Nathorst 1879a; Nathorst 1879b; Linnarsson 1880a; Linnarsson 1880b). Many of these early studies were concerned with determining the age of the rocks: Holm (1885) suggested a Triassic age based on the lithological similarity to the Triassic redbeds of southern Sweden, Nathorst (1886) proposed a Precambrian to early Cambrian age and Munthe & Gavelin (1907) believed in a Triassic age. As more evidences came to light, a Precambrian age became the most likely scenario: a fact that was pointed out by several authors (e.g. Rosén 1925; Brotzen 1941; Collini 1951). Recently the Visingsö Group was constrained to the Tonian Period within the Neoproterozoic era (Moczydłowska et al. 2017, see chapter 2.4).

The Visingsö Group have long been known to contain microfossils. Many of the earliest studies concerned the microfossil *Chuaria* (e.g. Linnarsson 1880b; Nathorst & Kramer 1884; Holm 1885; Brotzen 1941). Acritarchs were investigated by Ewetz (1932; 1933) and Timofeev (1960). Stromatolites from the Upper Formation were described by Vidal (1972). The acritarchs continued to be studied intensively in papers by Vidal (1974; Vidal 1976) and Knoll & Vidal (1980), and more recently by Mus & Moczydlowska (2000), Talyzina (2000), Loron & Moczydłowska (2017) and Moczydłowska et al. (2017). Brocks et al. (2016) described the biomarkers present in the Upper Formation.

Much of the recent palaeontological focus has concerned the so called vase-shaped microfossils and their emergence as an important biostratigraphical tool in the Neoproterozoic. Vase-shaped microfossils were first described by (Ewetz 1932) when they were found within phosphatic nodules of the Visingsö Group, and they were imaginatively described as 'single-celled organism with shell'.

2.2 The Neoproterozoic

The Neoproterozoic Era ranges from 1000 Ma until the start of the Cambrian Period at 541 Ma (Ogg et al. 2016). The era was preceded by the slow trudging evolution of microbial life and the earth's middle age; the 'Boring Billion' (Cawood & Hawkesworth 2014; Butterfield 2015). These apparently stable geological conditions and simple life forms were thrust into the turmoil of the Neoproterozoic and emerged on the other side with the first complex life forms (Butterfield 2015). The Neoproterozoic featured the famous 'Snowball-Earth' glaciations (Harland & Rudwick 1964; Kirschvink 1992; Hoffman et al. 1998), possibly the largest crustal-forming events ever (Rino et al. 2008), the formation of the Columbia and Rodinia supercontinents (Rogers & Santosh 2002; Li et al. 2008) and some of the most spectacular geochemical anomalies in Earth's history (Halverson et al. 2010).
The marine realm was stratified with free oxygen generally only found in the photic zone and productivity was largely confined to cyanobacteria (Butterfield 2015).

At the end of the Tonian Period (1000 - 720 Ma), the first signs of eukaryotes appear in the form of biomarker-evidence (Butterfield 2015). At this point there is a surge in evolution with the emergence of testate amoebae and 'scale microfossils' (Butterfield 2015; Moczydłowska et al. 2017). The oceans remained stratified through the Neoproterozoic with rising oxygen levels and high isotopic carbon values with distinct drops indicating a chaotic marine carbon cycle (Halverson et al. 2010). The end of the Neoproterozoic is characterized by high average $\delta^{13}C$ values (c. +5‰ compared to Mesoproterozoic and Phanerozoic values of c. 0 – 1‰), glacially related negative $\delta^{13}C$ excursions and negative $\delta^{13}C$ anomalies as of yet not connected to any glacials (Halverson et al. 2010). A substantial fractional burying of organic carbon is considered to cause the high average $\delta^{13}C$ (Hayes et al.

1999).

With the beginning of the Cryogenian (c. 720 Ma) the Neoproterozoic enter its hallmark icehouse conditions with glaciations potentially reaching tropical low-latitudes (Shields-Zhou et al. 2012). The negative $\delta^{13}C$ excursions are related to the Neoproterozoic glacials; the Sturtian (c. 715 – 680 Ma), Marinoan (c. 650 – 635 Ma) and Gaskiers (c. 579.63 – 579.88 Ma). The Sturtian and Marinoan are defined by their distinctive terminations of warm-climate 'cap-carbonates' overlying glacial tillites (Arnaud et al. 2011). The Bitter Springs anomaly is a distinct and globally correlated event that occurs at c. 810 Ma. It has been suggested to represent a change in organic carbon burial caused by the breakup of Rodinia which occurred around 850 Ma (Maloof et al. 2005; Li et al. 2008).

2.3 Formation and development of Baltica

Baltica (also known as the East European Craton) is composed of three distinct blocks: Fennoscandia, Sarmatia and Volga-Uralia (Bogdanova et al. 2008). They consist of archaen and Proterozoic crust that collided between 2.0 and 1.7 Ga (Gorbatschev & Bogdanova 1993). The Visingsö Group was deposited on the Baltic shield which is an area of the Fennoscandian block that roughly comprises present day Norway, Sweden and Finland (Fig. 1A).

The western parts of Baltica faced subduction zones (Rogers & Santosh 2002) as convergent tectonics caused several orogens (Bogdanova et al. 2008). These include the Gothian orogenic events (Gaál & Gorbatschev 1987), the Danopolonian Orogeny (Bogdanova 2001) and the Hallandian event (Hubbard 1975). After the Danopolonian orogeny and Hallandian event at 1.4 Ga various parts of western Baltica record extension and rifting in the form of within-plate mafic and bimodal magmatism (Åhäll & Connelly 1998).

The Sveconorwegian belt (Fig. 1B) is a ca. 500

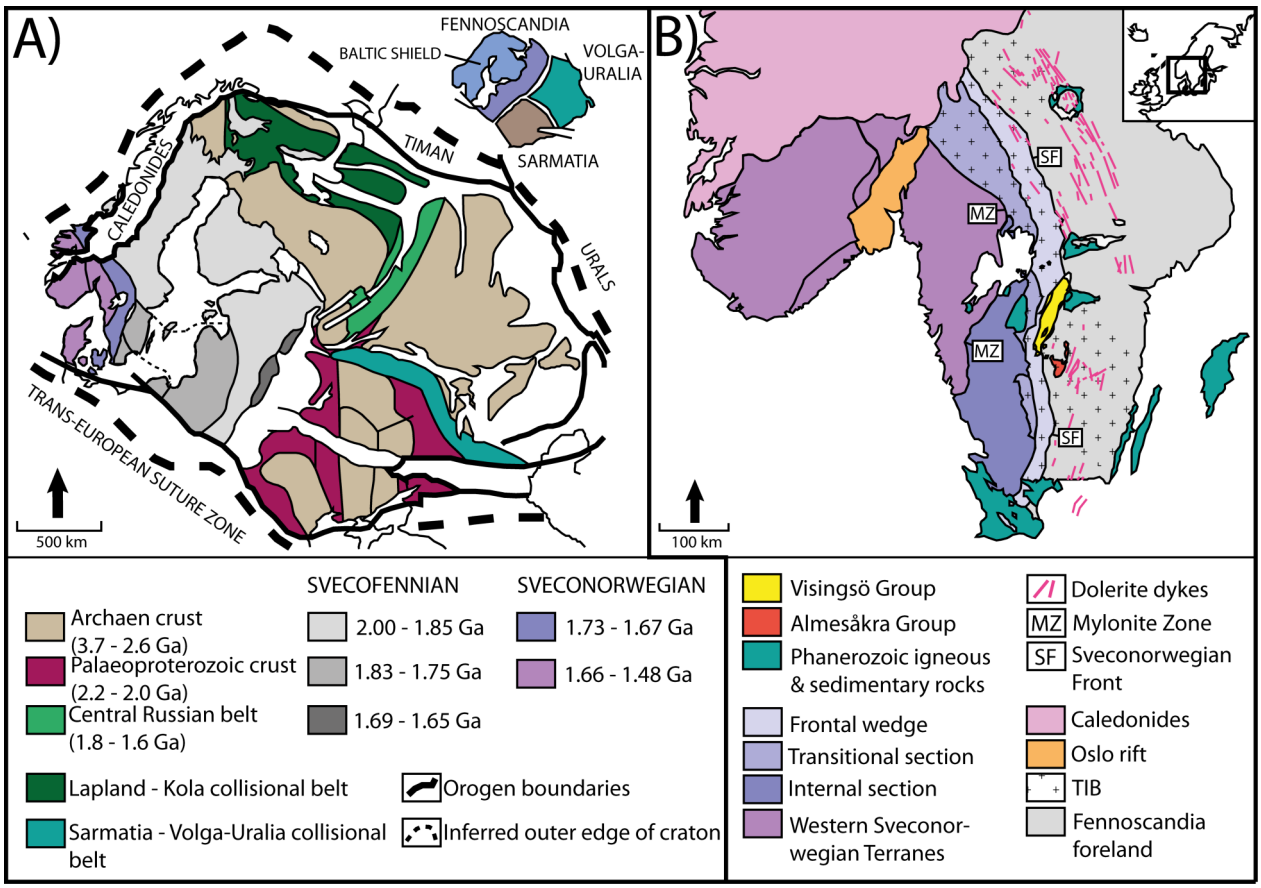

Figure 1. A: Tectonic map with ages of crusts and orogenic events in the East European Craton (EEC). The two collisional belts are Paleoproterozoic. Svecofennian and Sveconorwegian refer to corresponding domains. For the Sveconorwegian domain the ages represent initial crustal ages before the c. 1.13 – 0.97 Ga reworking during the Sveconorwegian orogeny. Modified from (Gee & Stephenson 2006; Bogdanova et al. 2008) B: Tectonic map of the Sveconorwegian orogeny. Fennoscandia foreland: 2.0-1.8 Ga (Möller & Andersson 2018). Transscandinavian Igneous Belt (TIB): 1.87-1.66 Ga (Möller & Andersson 2018). Overprint of Sveconorwegian orogeny (Blue hues): 1.14-0.92 Ga (Möller & Andersson 2018). Western Sveconorwegian Terranes: <1.65 Ga, occurrences of 1.05-1.02 granites and 0.98-0.92 Ga gabbro-granite not depicted in the map (Möller & Andersson 2018). Dolerite dykes: 0.97-0.94 Ga (Möller & Andersson 2018). Caledonides: 0.48-0.38 Ga (Möller & Andersson 2018). Oslo rift: 0.29-0.25 Ga (Larsen et al. 2008). Deposition of sedimentary groups: Almesåkra Group >0.97 Ga (Möller & Andersson 2018), Visingsö Group <0.88 Ga (Moczydłowska et al. 2017). Modified from Möller & Andersson (2018).

km wide belt of continental crust attached to the south-western parts of Fennoscandia that was subject to reworking during the Sveconorwegian orogeny between 1.13 – 0.97 Ga (Bingen et al. 2008). The Sveconorwegian orogeny is generally reconstructed in the Meso- and Neoproterozoic located adjacent to Laurentia as a part of the larger Grenvillian orogeny (c. 1250-980 Ma). The Grenvillian orogeny is linked to the assembly of the supercontinent Rodinia and today the rocks span large parts of eastern North America (e.g. Gower et al. 1990; Hoffman 1991; Torsvik et al. 1996; Karlstrom et al. 2001; Cawood & Pisarevsky 2006; Bogdanova et al. 2008; Cawood & Pisarevsky 2017; Merdith et al. 2017). The Sveconorwegian orogeny has been interpreted to either have formed through several accretionary events (Coint et al. 2015) or a collisional event (Bingen et al. 2008).

The Sveconorwegian belt consists of several lithotectonic units: the Fennoscandia foreland, the Eastern Segment and the Western Sveconorwegian terranes (Bingen et al. 2008). The Fennoscandia foreland mainly consists of the granitoids and porphyries of the Transcandinavian Igneous Belt (TIB) and Paleoproterozoic crust of the Svecokarelian (also known as Svecofennian) belt (Gorbatschev & Bogdanova 1993). The TIB was formed between 1850 Ma and 1660 Ma and is intruded by several plutons and dolerites (Bingen et al. 2008). The Eastern segment is the easternmost unit affected by the Sveconorwegian orogeny. It is composed of rocks of similar age and composition as the TIB but with a gneissic overprint (Söderlund et al. 1999; Söderlund et al. 2002; Högdahl et al. 2004). In progressing order from east to west are the remaining western Sveconorwegian terranes that have been transported relative to Fennoscandia: the Idefjorden terrane, the Kongsberg terrane, the Bamble terrane and the Telemarkia terrane (Bingen et al. 2008).

2.4 Age of the Visingsö Group

Magnusson (1960) conducted isotopic studies of detrital mica from the Visingsö group and the K-Ar data gave an age of 1060-985 Ma. Bonhomme & Welin (1983) dated whole-rock samples from the Upper Formation and acquired an Rb-Sr age of c. 706 - 663 Ma. They considered that this age represents a diagenetic event taking place after deposition which would give a minimum depositional age for the Upper Formation.

Microfossils and stromatolites from the Visingsö Group have been correlated with other geochronologically better constrained sedimentary groups. The age range based on these correlations falls between c. 800 – 700 Ma (Vidal & Moczydłowska 1995; Mus & Moczydlowska 2000; Moczydłowska et al. 2017). These sedimentary groups are the Hedmark, Vadsø and Tanafjord groups of the Norwegian Caledonides, the Thule and Eleonore Bay groups of Greenland, the Chuar, Uinta Mountains and Pahrump groups of western USA and the Little Dal, Mount Harper and Fifteen mile groups of Canada (Vidal 1976; Vidal & Ford 1985; Horodyski 1993; Vidal & Moczydłowska -Vidal 1997; Porter & Knoll 2000; Porter 2006; Nagy et al. 2009; Strauss et al. 2014; Moczydłowska et al. 2017). Moczydłowska et al. (2017) proposed a biostratigraphic minimum age of 740 Ma for the Visingsö Groups using acritarchs of the *Cycliocyrillium simplex* assemblage. Furthermore Moczydłowska et al. (2017) provided detrital zircon U-Pb ages from the Lower Formation that yielded a maximum depositional age for the Visingsö Group at 886 ± 9Ma. The zircon data together with the biostratigraphical minimum age placed the Visingsö Group within the age span 886 -740 Ma which corresponds to the Tonian Period (Moczydłowska et al. 2017).

2.5 Precambrian basins

The 'Jotnian' sandstones are various siliciclastic formations with ages spanning c. 1.6-0.9 Ga (Bingen et al. 2011; Lundmark & Lamminen 2016). A sedimentary group typically associated with the 'Jotnian' sandstones is the Almesåkra Group, located in an area southeast of Lake Vättern in the vicinity of the town Nässjö. The group consists of Middle Proterozoic sedimentary rocks deposited in a fluvial setting (Rodhe 1987). The formation is dominated by feldspathic arenites with subordinate argillites and conglomerates (Rodhe 1987). Dolerite magma intruded the rocks c. 1000 Ma (Patchett 1978; Söderlund et al. 2005). The mode of cementation for quartz and hematite in parts of the Almesåkra Group indicate a warm, arid to semi-arid palaeoclimate (Rodhe 1987). The group has seen moderate burial depths indicated by a low metamorphic grade of the argillites as well as by the authigenic mineralogy of the sandstones (Rodhe 1987). A fragment of the Almesåkra Group found within a conglomerate of the Visingsö Group provided the first evidence of the Visingsö Group being younger than the Almesåkra Group (Munthe & Gavelin 1907).

2.6 Lithology, stratigraphy and distribution

The rocks of the Visingsö Group are preserved as down faulted remnants within the vicinity of the Lake Vättern basin in south-central Sweden (Fig. 2A). The group consists of at least 1000 m of sedimentary rocks (Fig. 3B) and was subdivided into three major informal formations — the Upper, Middle and Lower formation — by Collini (1951). The deposition of the sediments is tied to the aftermath of the Sveconorwegian orogeny when post-orogenic relaxation created extensional tectonism that facilitated the creation of a sedimentary basin (Larsen & Nørgaard-Pedersen 1988). The different informal formations are believed to represent different stages of the development of a rift basin (Larsen & Nørgaard-Pedersen 1988).

The Lower Formation is a fluvial-deltaic succession dominated by quartz arenites with minor constituents of mud and coarser sediments (Collini 1951; Vidal 1974; Persson et al. 1985; Larsen & Nørgaard-

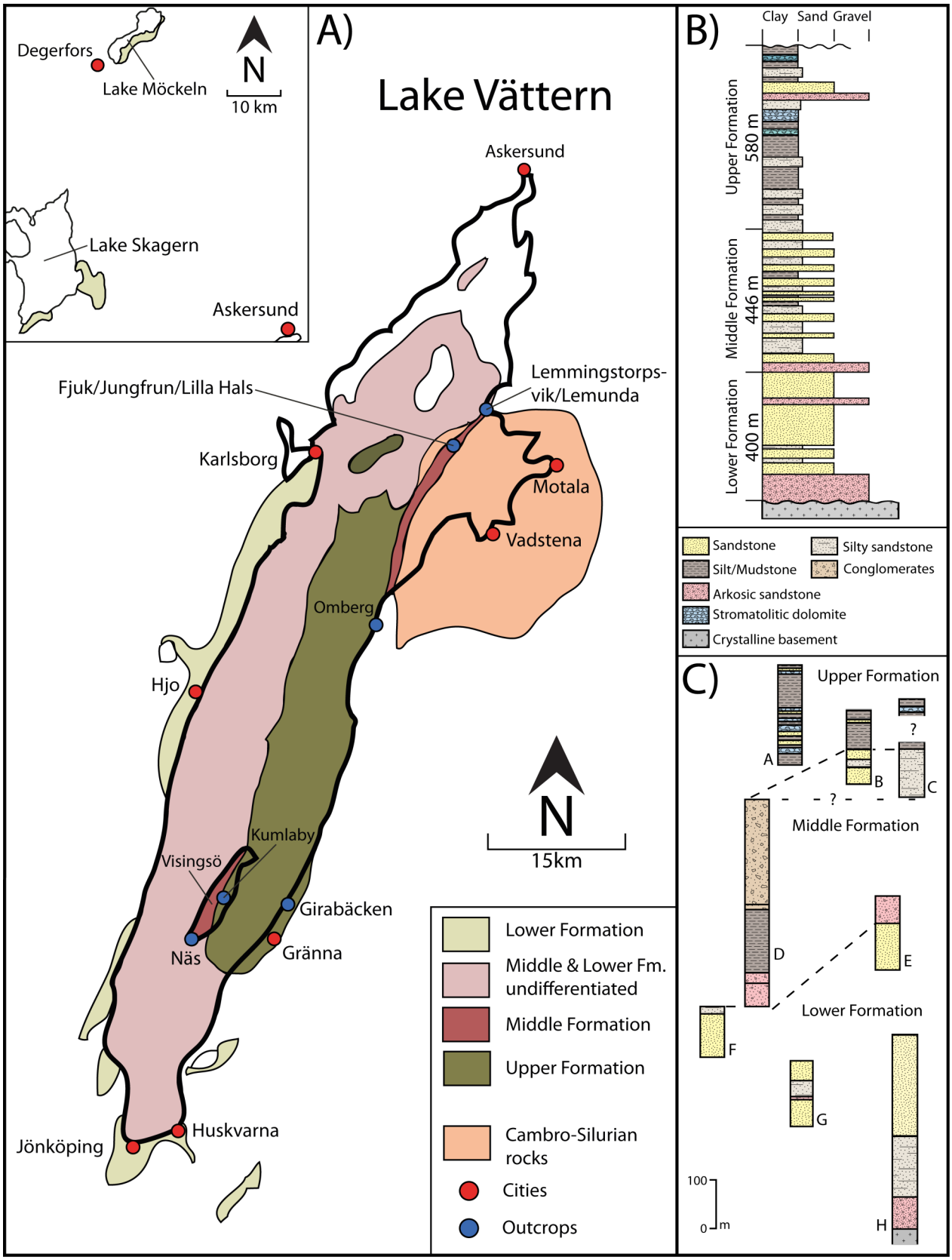

Figure 2. A: The distribution of the Visingsö Group in the Lake Vättern area. Modified from Axberg & Wadstein (1980). B: Lithology and stratigraphy of the Visingsö Group. Modified from (Moczydłowska et al. 2017). *C:* Tentative lithostratigraphic correlation of the Visingsö Group: A: Omberg (Vidal 1985). B: Kumlaby (Visingsö) borehole (Collini 1951). C: Visingsö. Includes the sections located at Näs and additional outcrop*s* further north along the coast (Collini 1951; Vidal 1976). D: Lemmingstorpvik + Lilla Hals (Vidal & Bylund 1981). E: Girabäcken (Brotzen 1941). F: Lemunda (Vidal & Bylund 1981). G: Karlsborg borehole (Vidal 1974). H: Huskvarna borehole (Brotzen 1941). Modified from Larsen & Nørgaard-Pedersen (1988)

Pedersen 1988). The sandstones are medium- to coarse grained and white, yellow or red coloured (Vidal 1974). The thickness of the unit was estimated to 145m by Collini (1951), however gravimetric data in the southern parts of the Lake Vättern area points to an at least local thickness of 400m (Lind 1972). Boreholes from the Huskvarna and Jönköping areas gave thicknesses of 176 m and in the Karlsborg area 195m (Fig 2C; Vidal 1974). The formation is accessible in outcrops in the Girabäcken valley, southern Omberg, Lemunda, small outcrops in the southwestern parts of Lake Vättern and around the lakes of Möckeln and Landsjön (Fig. 3A; Vidal 1974). The boundary between the Lower- and Middle Formation can be seen in the Girabäcken valley where quartz arenite is overlain by a porous, red coloured silty sandstone and conglomerates (Vidal 1974).

The Middle Formation records the transition into a half graben setting and contains shales, siltstones, sandstones, arkoses and conglomerates with lithologies of a bimodal sedimentological origin. The sediments have been inferred to be deposited as delta lobes prograding into a shallow marine setting (Collini 1951; Vidal 1976; Persson et al. 1985; Larsen & Nørgaard-Pedersen 1988). The Middle Formation is exposed in four areas; the Näs outcrops, Girabäcken, the Lemunda peninsula and on the small islands of Jungfrun and a group of small islands called Fjuk in northeastern Vättern (Fig. 3A; Larsen & Nørgaard-Pedersen 1988). Spectacular conglomerates, with boulders measuring 12m x 8m x 10m, referred to as Lilla Hals boulder beds outcrop in coastal exposures at Lilla Hals as well as on Jungfrun and Fjuk (Fig. 3A; Vidal & Bylund 1981). The conglomerates consist of polymict boulders of gneissic, porphyritic and granitoid crystalline rocks. The matrix consists of coarse feldspathic sand supported by limonitic cement. Vidal & Bylund (1981) considered the Lilla Hals boulder beds to be deposited through debris flows in a graben setting.

Exposures of the Upper Formation can be found in the central and eastern parts of the Vättern basin such as on the island of Visingsö, in the Girabäcken valley and north and south along the coastline in the vicinity of the town Gränna (Fig. 3A). The boundary between the Middle and upper Upper Formations is said to be gradual but the exact relationship is not yet determined. Collini (1951) placed the boundary where mudstones began to be dominant in the outcrops northeast of Näs on the island of Visingsö. The Upper Formation is dominated by dark silty mudstones with dolomitic limestone and stromatolites. Beds of conglomerates and sandstones are subordinate and the depositional environment is thought to have been shallow marine with episodes of subaerial exposure and storm/tidal activity (Vidal 1972; Vidal 1976; Persson et al. 1985; Larsen & Nørgaard-Pedersen 1988).

2.7 Diagenetic history

The Visingsö Group have been subjected to diagenesis but very little metamorphism. According to Morad (1983b) the diagenesis unfolded during three arbitrary stages.

The early stage is related to shallow burial with relative low pressure and temperature. Compaction had begun and the position of the water table determined the reactions that were mainly oxidation and reduction (Morad 1983b). Thermodynamically unstable particles were dissolved into cations or altered into clay minerals with feldspars being a plausible source for the cations (Morad 1983b). Chloritization and the formation of pyrite occurred frequently, the latter mainly in the Lower and Middle formations(Morad 1983b). Oxidation facilitated the development of hematite in the sandstones of the Lower Formation and lowest part of the Middle Formation and illite and leucoxene formed from altered biotite (Morad 1983b). Early authigenic clay minerals included chlorites and mixed-layer illite-montmorillonite (Morad 1983b). Arkoses and feldspathic sandstones from the Middle and Upper formations were often cemented by authigenic coarsely crystalline calcite displaying a poikilotopic texture. This is considered as an indication of loose packing of grains within an environment of shallow burial with high permeability and porosity (Morad 1983b). Precipitation in the pore space took place through fine-grained chlorites and, whenever the environment was acidic, kaolinite (Morad 1983b).

The intermediate stage saw an increase of burial depth with resulting higher temperature and pressure that led to closer packing of the grains (Morad 1983b). A pseudo-matrix is thought to have formed in the sandstones and arkoses of the Middle Formation through plastic flow of softer particles (Morad 1983b). Pressure-solution commenced and dissolved silica formed authigenic overgrowths on detrital quartz. The resulting cementation led to a loss of porosity and permeability (Morad 1983b). Calcite filled the remaining pore space and replaced interstitial clay and some of the quartz overgrowths (Morad 1983b).

The reactions of the late diagenetic stage resemble those of closed diagenetic systems. A loss of porosity and permeability decreased the role of circulating pore solutions and instead pressure and temperature were the main factors controlling diagenesis (Morad 1983b). Hydromuscovite formed in remaining interstitial space (Morad 1983b).

2.8 Tectonic setting

The orogen-parallel Sveconorwegian Front defines the extent of Sveconorwegian reworking and acts as the boundary between the Eastern Segment and the Fennoscandia Foreland (Fig. 1B). In the literature the Sveconorwegian Front is also referred to as the Protogine Zone and the Sveconorwegian Frontal Deformation Zone, which defines the areas south and north of Lake Vättern respectively (Andréasson & Rodhe 1990; Wahlgren et al. 1994). Ductile shear zones with-

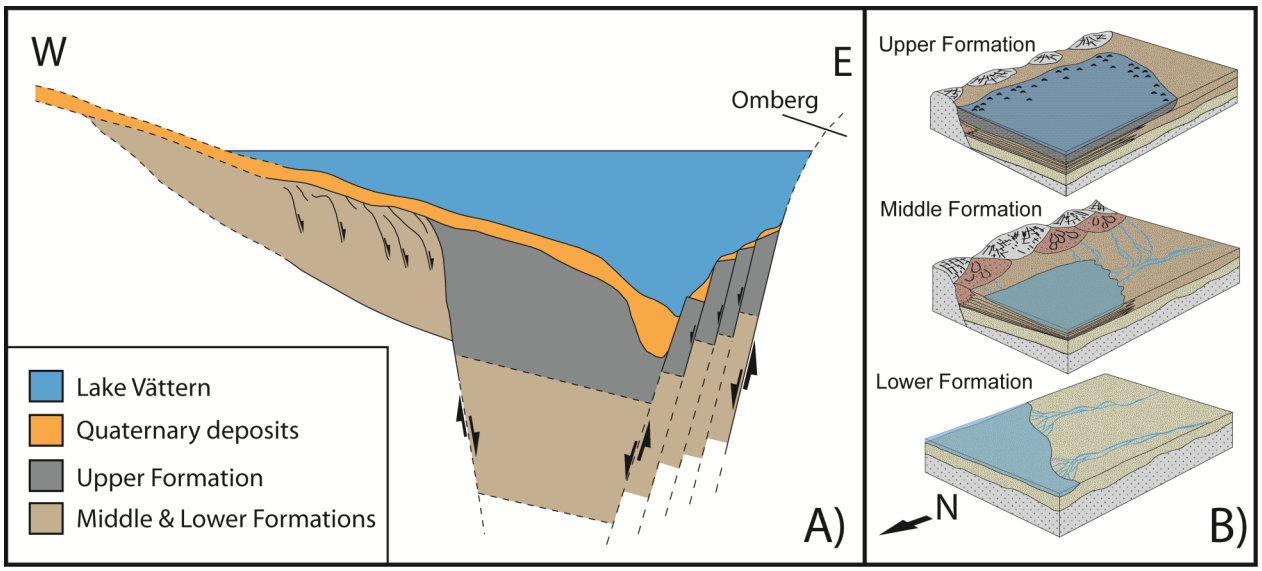

Figure 3. A: Tectonic model for the lake Vättern basin based on seismographic data. Modified from Axberg& Wadstein (1980) B: Sedimentary and tectonic development of the lake Vättern Basin. Modified from Larsen & Nørgaard-Pedersen (1988).

in the Sveconorwegian Front have been dated using $^{40}Ar/^{39}Ar$ plateau ages of muscovite. These indicate activity between 964 ±1 to 905 ±5 Ma (Andréasson & Dallmeyer 1995; Page et al. 1996).

Bimodal magmatism is associated with crustal thinning and rift settings (Brewer et al. 2004). Two such pulses have been identified in association with the Sveconorwegian Front and they were dated to c. 1220 and 1200 Ma, which indicates that the area has been a zone of weakness since at least the Mesoproterozoic (Söderlund & Ask 2006). Fennoscandia was subject to many instances of rifting and failed continental breakups in the Tonian related to the instability of Rodinia (Kumpulainen & Nystuen 1985). The crustal instability created fractures trending north-northwest, north and north-northeast on the craton (Andreasson et al. 1987). Ductile shear zones within the Lake Vättern area have a brittle deformational overprint. This deformation is possibly related to tectonic activity in the Permian and the tectonism within the Lake Vättern area could therefore be analogous to the Oslo rift (Agneta Månsson-Clausen, personal communication)

The three formations of the Visingsö Group likely reflect successive tectonic stages in the development of an extensional basin (Fig. 3B). The first stage included deposition of the Lower Formation in NE-SW trending fracture lineaments on a Precambrian peneplain (Martin 1939). The Lower Formation was deposited on top of a weathered kaolinized basement consisting of granitoids in an area larger than the present day Vättern trench, evident by the presence of rocks belonging to the Lower Formation around Lake Möckeln and Skagern (Collini 1951). The Middle Formation was deposited in a half-graben setting with syntectonic sedimentation of breccia's and conglomerates of the Lilla Hals boulder beds (Vidal & Bylund 1981; Larsen & Nørgaard-Pedersen 1988). The Upper Formation show few signs of syntectonic deposition implying that at least major tectonic changes had ceased at the time (Collini 1951; Vidal 1976). Larsen & Nørgaard-Pedersen (1988) inferred that the Middle Formation was deposited in a half graben-setting based on the immaturity of the sediments coupled with the geographical distribution of the different formations (Fig. 3A). The rocks in the southern parts of the basin belong to the Lower Formation, whereas the Middle and Upper formations are preserved in the deeper eastern part (Norrman 1964). The NE-SW faulting is thought to be the beginning of the major fault event that resulted in the deposition of the Middle Formation (Larsen & Nørgaard-Pedersen 1988). The rock sections on the eastern side of Vättern, in the vicinity of the town Gränna, show a repeated fault pattern that indicates that the half-graben was reactivated after their deposition. This reactivation could possibly have taken place in the tectonically active Permian or more recently due to Quarternary uplift (Larsen & Nørgaard -Pedersen 1988)

2.9 Study area

The studied outcrops are located in the vicinity of the 12th century royal residence 'Näs fortress' which lies at the southern tip of the island of Visingsö (Berg 1872). The island itself is located within the southern parts of Lake Vättern which in turn lies centrally in the southern parts of Sweden (Fig. 4). The outcrops follow the shoreline east and northeast of the fortress and consist of four individual outcrops that were divided into three sections. Some parts of the shoreline can be accessed from the mainland relatively simply but in order to investigate all of the sections one needs to wade, climb the steep cliffs or use a boat. Section 1A + 1B and the western parts of section 2 can be reached by a descent at Näs fortress and then a hunched walk along the artificial wave-breaker. The eastern parts of section

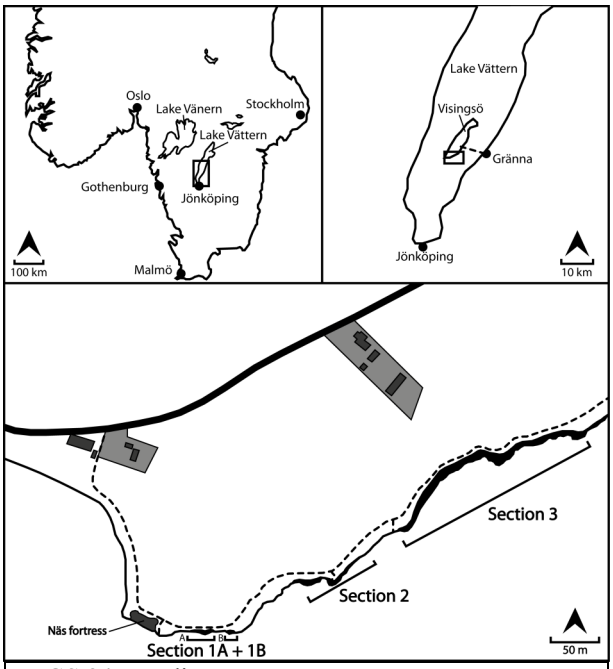

WGS 84 coordinates	
Section 1A+B	N57° 59.878, E014° 17.526
Section 2	N57° 59.911, E014° 17.676
Section 3	N57° 59.984, E014° 17.865

Figure 4. Location of the studied oucrops and their corresponding sections in the vicinity of 'Näs fortress' on the southern tip of the Island of Visingsö in south-central Sweden and GPS coordinates for the sections.

2 and the most westerly parts of section 3 can be reached by descending at the place of a lonesome juniper tree. Another descent is possible close to the most westerly parts of section 3. In order to reach most of section 3 one needs to brave the cold waters of Lake Vättern or perform an assisted climb down the steep cliffs.

The outcrops studied in this paper extends for about 200 m along the coast and the measured sections represents c. 28 m of sediments in total. The total lateral extent of the outcrops on south eastern Visingsö measures c 3.5 km aided by the fact that the sediments have a dip of c. 5-10° ESE (Larsen & Nørgaard-Pedersen 1988). The outcrops along the coastline represent a large part of the Middle Formation and the lower part of the Upper Formation (not included in the map), the sections studied herein only cover the Middle Formation. No contacts between the formations are apparently exposed in the area (Larsen & Nørgaard-Pedersen 1988). The beds have a plane parallel appearance, top layers can sometimes be disturbed by glacial tectonics and some beds are in a few places disturbed by the vertical faults running through the outcrops. Several bedding planes are present with various features such as microbially induced sedimentary structures, ripple marks and desiccation cracks.

3 Material and methods

3.1 Stratigraphy and lithology

Fieldwork took place in several instances throughout 2017 and 2018. The stratigraphic log was produced by centimetre scale measurements of the outcrops. Notes were taken regarding the overall lithology, sedimentary structures and colouration. Samples were taken continuously throughout the sections from various lithologies to produce petrographic thin sections and for detrital zircon sampling. Samples of the different lithologies were cut, polished and embedded in epoxy in order to produce thin sections using a manual whet machine.

3.2 Geochronological sample preparation

Three samples were chosen for detrital zircon analysis. Sample #306 at 7.05 m in Section 3, Sample #308 at 7.5 m in Section 3and Sample #312 at 18.85 m in Section 3. The samples were crushed and then ground in a steel mill. Heavy minerals were separated using a Wifley shaking-table using the techniques outlined in Söderlund & Johansson (2002). Magnetic minerals were removed with a handheld magnet and the zircons were hand-picked under a binocular microscope. 150 grains was selected from each sample. Care was taken to try and pick a wide array of morphologies and sizes and hence 75 small zircons and 75 large zircons were chosen from each sample..

The zircons were placed on double-sided tape and cast into ~2.5 cm wide cylindrical epoxy mounts. These mounts were polished to expose a cross-sections of the zircon crystals in order to determine grain morphology and placing spots for Laser-ablation analyses both cathodoluminescense (CL) and backscattered electron (BSE) images were produced. These were made with the Tescan Mira3 High Resolution Schottky FE-SEM located at the Department of Geology at Lund University.

3.3 U/Pb isotope analyses

U-Pb isotope analyses were performed using the LA-ICP-MS system available at Lund University (See table 1.); this system uses a Teledyne Photon Machines G2 laser coupled to a Bruker Aurora Elite quadrupole ICP-MS. The instrument tuning uses NIST612 and aims to obtain high and stable signal counts on: uranium and lead isotopes, low oxide production ($^{238}U/^{238}U^{16}O$ < 0.5 %) and Th/U ratios around 1.

Laser power was measured directly in the sample cell through the use of an energy meter. The analytical sessions ran automatically with standard-sample-standard bracketing, using GJ1 (Jackson et al. 2004) as primary standard and with 91500 as secondary standard (Wiedenbeck et al. 1995). The analyses used 300 shots at 10 Hz and fluency between 2.5 and 3 J/cm^2. Baseline compositions were measured for 30

Table 1. LA-Q-ICP-MS methodology Lund University

Laser ablation system	
Make, Model & type	Photon machines, Analyte G2 excimer laser
Ablation cell & volume	HelEx 2 sample cell
Laser wavelength	193 nm
Pulse width	<4 ns
Fluence	2.5 to 3 J/cm^2
Repetition rate	10 Hz
Spot size	20x20 µm
Carrier gas	He as carrier gas. Ar and N2 make-up gas combined down-stream from sample chamber using a Y-connector.
Background collection	30 seconds
Ablation duration	30 seconds
Wash-out delay	3 seconds
Cell carrier gas flow	0.8 l/min He and 6.5 ml/min N2
ICP-MS Instrument	
Make, Model & type	Bruker Aurora Elite Quadrupole ICP-MS
Sample introduction	Via conventional tubing with insert "squid"
RF power	Ca. 1300 W
Make-up gas flow	Ca. 1 l/min Ar
Detection system	Single collector discrete dynode electron multiplier or DDEM
Masses measured (dwell time in milliseconds)	^{202}Hg(10), ^{204}Pb(25), ^{206}Pb(15), ^{207}Pb(25), ^{208}Pb(10), ^{232}Th(10), ^{238}U(10)
Total scan time	120 milliseconds
Data Processing	
Gas blank	20 second
Calibration strategy	GJ1 as primary standard reference, 91500 as secondary standard reference
Reference Material info	Jackson, S. et al. (2004). Chem. Geol. 211, 47–69. Wiedenbeck, M. et al. (1995). Geostandard Newsletter, 19, 1-23.
Data processing	Iolite software (Paton et al. (2011). G Cubed, 11, doi:10.1029/2009GC002618)

seconds before each measurement and subtraction was done with a step-forward approach.

Common Pb was monitored by measuring ^{202}Hg and mass 204 (^{204}Hg+^{204}Pb). Mass 204 baseline levels measured c. 1100 cps with a standard error (SE) around 30 CPS (~2-3 %). The common Pb monitoring was based on inspection of the raw counts during reduction of data and on baseline subtracted ^{206}Pb/^{204}Pb CPS ratios. Data reduction was performed with the software Iolite using the X_U_Pb_Gerchron4 DSR (Paton et al. 2010; Paton et al. 2011)

3.4 Zircon morphology

The collected zircons are of varied size, morphology and internal structure with colours ranging in various yellow hues from almost clear to dark yellow. The size of the grains ranged between c. 50 – 150 µm on their C -axis. Based on their morphology the zircons were divided into two groups: rounded and angular (Fig. 5A -E).

The rounded grains displayed morphologies ranging from circular (Fig. 5A) to ovoid (Fig. 5B) and oblong (Fig. 5C). They consistently showed signs of homogenous inner structures or recrystallization. Some outliers retained clearly discernible cores and

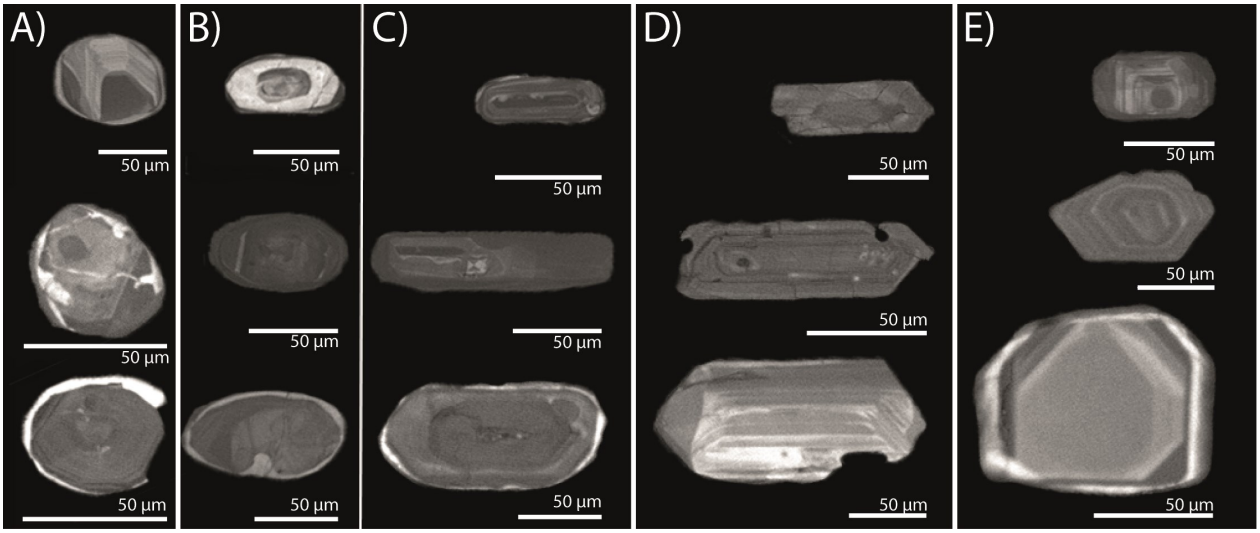

Figure 5. Cathodoluminesence images of representative grains for morphological groups of Zircons identified within the Näs sections. A: Rounded group circular morphology. B: Rounded group ovoid morphology. C: Rounded group oblong morphology. D: Angular group prismatic crystal structure. E: Angular group pyramidal crystal structure.

oscillatory zoning. CL imaging revealed lighter rims on the edges of many grains. Inclusions were common and occasional xenocrystic cores and inclusions occurred. Fractures appeared along both the length and width of the grains. Furthermore the fractures often appeared along borders between individual oscillatory zonations and in particular along outer rim layers.

The angular grains displayed both prismatic (Fig. 5D) and pyramidal crystal terminations (Fig. 5E) . The majority of the angular grains displayed clear inner structures such as oscillatory zonation and distinct cores in CL imaging. A few grains displayed reworked oscillatory zoning. Fractures were common and some of the grains hosted inclusions. Some fractures protruded radially from distinct cores, as if the grains were damaged by metamictization. Others went straight through the grains without any clear orientation. Inclusions and xenocrystic cores occurred in some of the grains.

4 Results

4.1 Lithofacies

4.1.1 Lithofacies M – Mudstone

The Mudstone lithofacies is distinguished by a laminated dark grey mudstone containing clay, silt and fine sand sized grain-fractions (Fig. 6A; 7c). In some parts the differing grain sizes constitute individual fine laminae. The Mudstone lithofacies can be found in all studied sections and it occurs throughout them as well as terminates several sections.

The Mudstone lithofacies occurs as a dark laminated shale and with heterolithic structure indicative of deposition within a depositional setting with differing energy levels, inferably tidal currents. The sandy portions of the heterolithes differs in their compostion. The majority belongs to a fine-grained, well-sorted, rounded quartzitic sandstone. Overall the sand components are poorly consolidated with virtually no cementation. Some intervals within lithofacies M have a distinct rust-coloured appearance.

Lithofacies M displays a variety of bedding features such as lenticular, wavy and flaser bedding. Wavy bedding is the dominating bedding feature within the heterolithes. The sand lenses are predominantly connected and a few centimetres thick.

4.1.2 Lithofacies S – Siltstone

Lithofacies S consists of clay, silt and fine sand with silt being the dominant grain fraction. Lithofacies S is the most common lithofacies within the studied interval and it occurs throughout the four studied sections. Individual beds vary in thickness from centimetre to metre scale. The beds commonly have a blue-green-greyish appearance (Fig. 6B). Distinct layers with red-purple colouration occur throughout the sections. The rocks commonly exhibit a varying amount of fissility that is less well developed than the laminations of lithofacies M.

Few sedimentary structures can be seen within the Siltstone lithofacies. Some intervals contain faint ripple-like structures and desiccation cracks and the fissility sometimes takes on a wavy or undulating appearance. The siltstone often follows the mudstone as a part of continuous increase in grain size. The boundaries towards mudstones are often sharp and towards coarser sediments the boundaries are both gradual and sharp.

4.1.3 Lithofacies QGW – Quartz greywacke

Lithofacies QGW consists of a greywacke with a ma-

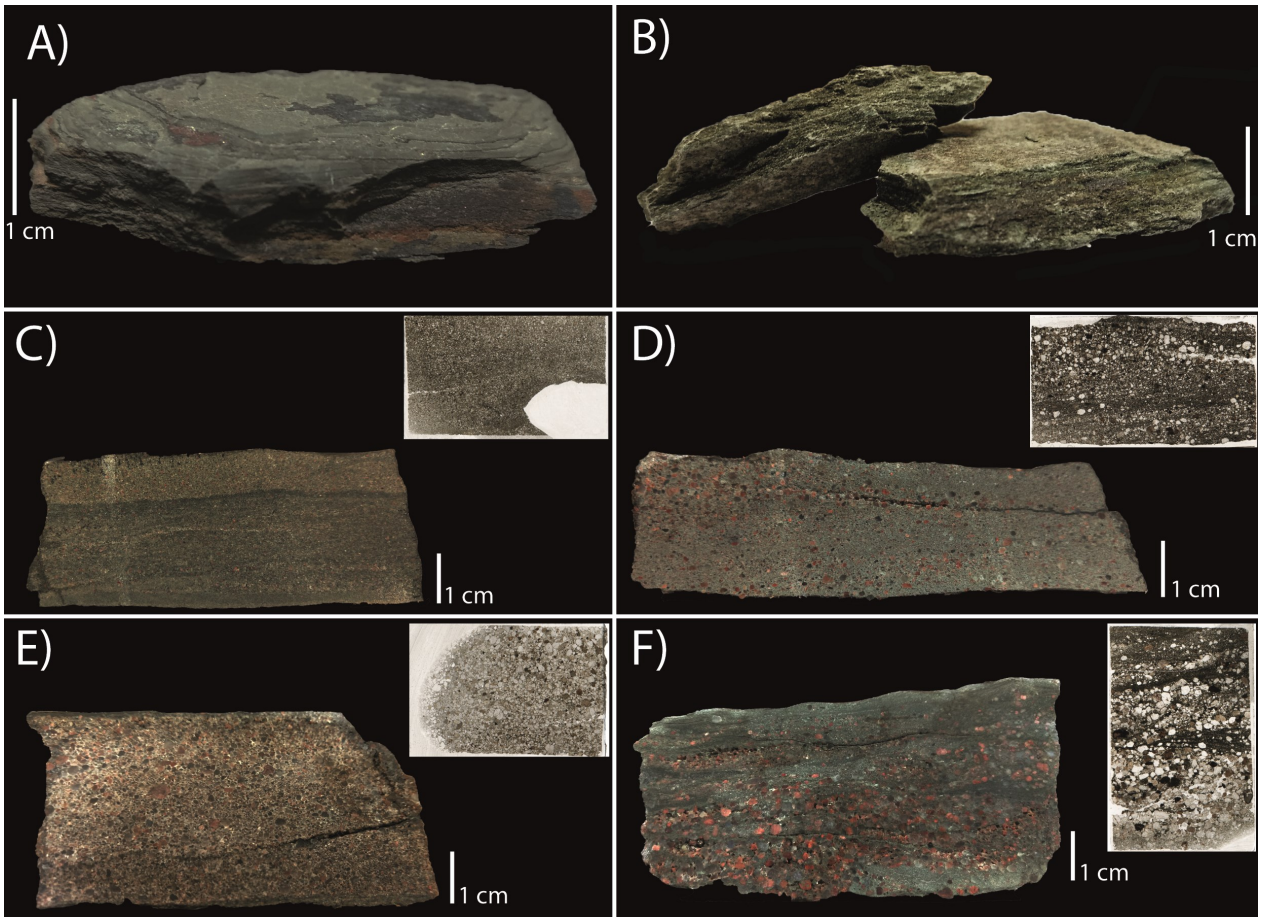

Figure 6. Images of the identified lithofacies of the Näs sections with thin-sections where they were possible to produce. A: Mudstone (Lithofacies: M) B: Siltstone (Lithofacies S) C: Quartz-Greywacke, note damage of thin section during preparation. (Lithofacies: QGW) D: Arkosic-Greywacke (Lithofacies: AGW) E: Subarkosic-Sandstone. Note uneven abrasion of the thin section. (Lithofacies: SST) F: Arkosic sandstone occurring within a fine grained matrix. (Lithofacies: AST).

trix of both clay and silt and the total matrix constitutes between c. 60 - 90% of the rocks. The colour of the rocks range between: green, blue and grey (Fig. 6C). Some intervals display red to purple colours. The framework grains consist of well sorted quartz grains and with subordinate feldspar grains, mainly in the fine to medium size range. The roundness of the grains range from being angular to well rounded. Some of the rocks display a faint sorting of grain sizes but overall the rocks display very few structures and appears massive.

The Quartz Greywacke occurs in all studied sections and is often found in conjunction with the siltstone lithofacies that it follows stratigraphically with a transitional boundary. Very few sedimentary structures have been found within Lithofacies QGW, some poorly developed cross bedding and possible ripple marks exist but overall the rocks have a massive appearance with little indication of any dominant sorting processes involved in the deposition.

4.1.4 Lithofacies AGW – Arkosic greywacke

The matrix of the Arkosic Greywacke consists of clay and silt that makes up c. 40% - 90% of the total amount. The sand fractions range from fine to coarse sand and are moderately to poorly sorted. The grains range from rounded to angular and consist of quartz and feldspar. The rocks vary in colour from a green – grey – blueish variant to a red – purple (Fig. 6D). Lithofacies AGW is a common occurrence in sections 2 and 3 but is absent from section 1. Some sedimentary structures can be distinguished such as faint foresets, wavy bedding, ripples and desiccation cracks. In thin sections the arkosic greywacke lithofacies often displays thin dark laminae resembling small ripple structures. Some grain size sorting occur within the rocks as some lamina contains more coarser feldspar rich constituents.

4.1.5 Lithofacies SST– Subarkosic sandstone

The Subarkosic Sandstone is well cemented and dominated by quartz with minor constituents of feldspar. Weathered rocks display a yellow colour and freshly cut they have a dark grey-green appearance (Fig. 6E;). Lithofacies SST has virtually no matrix and the mod-

Figure 7. Prominent outcrop (c. 9m high) in section 3. B: Cyclic deposition of siltstone, greywackes and sandstones. Section 2. C: Heterolithic mudstone, section 3. D: Tempestite from section 2 displaying clear horizontal lamination. E: Hummocky cross-stratification of a sandstone in section 3. F: Possible Microbially induced sedimentary structure in the topmost part of section 1. G + H: Well developed desiccation cracks in section 3. Photos: Ahrenstedt, Lindskog.

erately sorted grains range from fine to medium coarse sand. The grains are very well compacted with signs of pressure-dissolution and their morphology range from sub-angular to rounded. Lithofacies SST is absent from section 1 but occurs in sections 2 and 3. It is moderately sparse compared to other Lithofacies but increases in frequency higher towards the final stages of section 3. The Subarkosic sandstone is the lithofacies that displays the most abundant and well developed sedimentary structures within the studied sections. These sandstones display laminated bedding (Fig. 7D), trough-cross-bedding (Fig. 7E), desiccation cracks (Fig. G-H), ripple structures and mud drapes. Many beds have sharp lower and upper contacts indicating an erosional deposition. They are often overlying the greywackes and overlain by coarser more feldspar rich sediments. The Subarkosic Sandstones display either partial or entire sets of classical tempestite

structures such as parallel lamination, erosional surfaces or hummocky cross stratification (Brenchley 1989).

4.1.6 Lithofacies AST– Arkosic sandstone

The Arkosic Sandstone consists of fine to coarse grained sandstone with sub-rounded to angular grains. The beds often have a reddish appearance due to the high amount of feldspar, this is coupled with an underlying green-blue matrix resembling that of the Subarkosic Sandstone and the greywackes (Fig. 6F). The amount of feldspar varies from rocks being almost completely built up of feldspars to rocks verging on the border of being subarkosic. The total amount of individual beds that are Arkosic Sandstone are few but they do occur in all three sections and often within other lithofacies: for instance the Arkosic Greywacke is probably a product of intermingling between the sediments making up the Quartzitic Greywacke and the Arkosic Sandstones. The Arkosic Sandstone is often found in conjunction with the Subarkosic Sandstone where it usually overlies the less feldspar rich sandstones as part of a coarsening upward cycle. They often terminate individual coarsening-upwards cycles with centimetre thin feldspar layers of conglomerate-like intervals containing abundant ripple structures (Such as at 8.85 m in section 3). Sharp wavy contacts towards underlying beds are a common feature for lithofacies AST. Cross lamination occurs but most often the sediments have a very massive appearance.

4.2 Cycles and depositional trends

The sedimentology of the Näs sections are defined by coarsening-upwards cycles coupled with an increasing feldspar content. These cycles consist of a lower part with Mudstone- or Siltstone Lithofacies, followed by Arkosic- and Quartz Greywacke Lithofacies, which in turn is followed by the Subarkosic Sandstone Lithofacies and the Arkosic Sandstone Lithofacies respectively. The cycles are then terminated by sediments containing bathymetric indicators of either tidal influence or subaerial exposure.

Throughout Sections 1A+B, Section 2 and the lower half of Section 3, these cycles are terminated by the heterolithic mudstone of Lithofacies M and represents deposition in a foreshore/intertidal setting (Martin 2000). Throughout the later parts of section 3 the coarsening-upwards cycles are terminated by mud-drapes that are associated with tidal settings (Allen 1981) and deposition above the Fairweather wave-base (FWWB). The desiccation cracks found throughout Sections 1A+B and Section 2 imply subaerial exposure and deposition above the FWWB (Corte & Higashi 1964). No evaporites have been found ruling out an arid environment with significant evaporation (Sonnenfeld 1984). The Subarkosic sandstone Lithofacies were deposited as tempestites and indicate deposition between the Storm Wave Base (SWB) and the FWWB (Harms 1975). The Siltstone Lithofacies represents deposition below or near above the SWB (Tucker 2009).

Section 1A (Fig. 8) mainly consists of Siltstone Lithofacies deposited below the Storm-wave base (SWB). When simplified the section becomes one coarsening upwards cycle with deposition above the fair-weather wave base in the last metre of the section. The only bathymetric indicators located within Section 1A are the desiccation cracks found close to the top of the section. Minute structures possibly being of organic origin also occur at this level. Section 1B (Fig. 8) starts with what resembles a small coarsening-upwards cycle that is terminated at about 0.1 m by heterolithic structures. This is however not a typical heterolithic mudstone but more resembles the surrounding greywackes. The remainder of Section 1B belongs to one complete coarsening-upwards cycle that terminates at the end of the section. The first metre was mainly deposited below the SWB in the form of Siltstone before moving into alternating with deposition above the SWB with the greywackes and tempestites. The cycle terminates with heterolithic mudstone deposited above the FWWB in the last centimetres.

Section 2 (Fig. 9) starts with what appears to be the later parts of a coarsening-upwards cycle from 0 – c. 1.5 metres. This partial cycle consists of two smaller individual coarsening-upwards cycles before a fining upwards trend with greywackes and sandstones being followed by siltstone and then terminating in a heterolithic mudstone. The mudstone is followed by sandstone containing desiccation cracks that in turn is followed by a coarsening- upwards sequence that occupies the reminder of section 2 and terminates with several layers containing desiccation cracks and a heterolithic mudstone.

Section 3 (Fig. 9-12) begins with three coarsening-upwards cycles that are each terminated by heterolithic mudstone. They are characterized by cyclic deposition of siltstone, greywackes and tempestites. The first cycle terminates at 3 metres, the second cycle ranges from c. 3-5 metres and the last cycle ranges from c. 5.5-7 metres (Fig. 9-11). The last cycle is dominated by siltstone with coarse material in its later stages. The remaining c. 13 metres of section 3 (Fig. 11, 12) see a change in the framework of the cycles as they are terminated by mud drapes instead of heterolithes. Throughout these 13 metres there are several coarsening-upwards cycles and sandstones become more common and individual beds becomes larger and displays clear tempestite structures.

4.3 Detrital zircon U/PB-ages

Sample 306 yielded U/Pb ages with age peaks at: 1.84 Ga, 1.8 Ga, 1.75 Ga, 1.7 Ga, 1.65 Ga, 1.61 Ga, 1.48 and 1.04 Ga (Fig. 13). No weighted mean could be produced to determine the maximum depositional age for sample 306 as there was no youngest group of zircons, only a single zircon with an age of 1048 ± 5.7

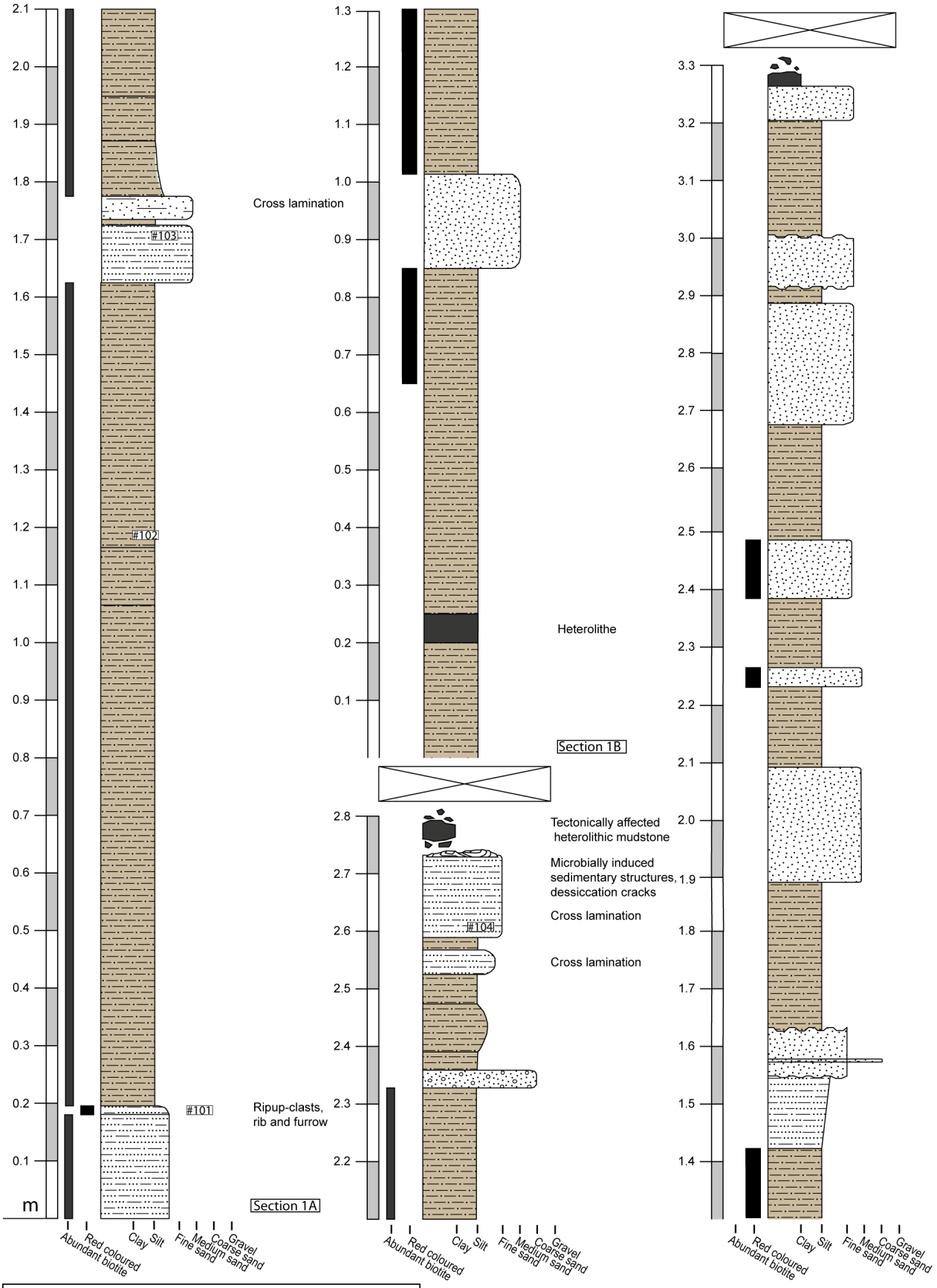

Figure 8. Stratigraphic log from the Näs locality showing section 1A (0 – 2.8m) and section 1B (0 – 3.3m)

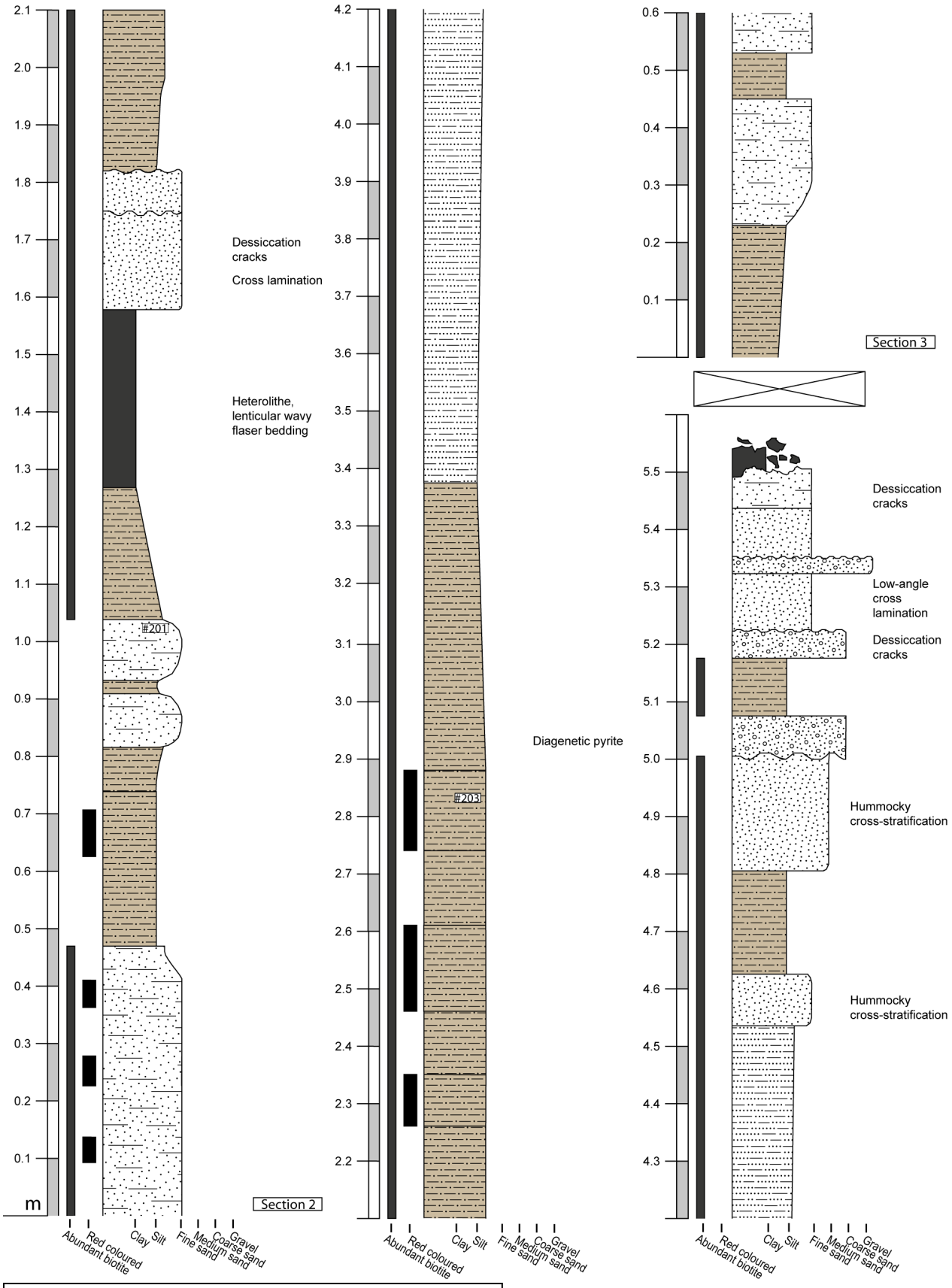

Figure 9. Stratigraphic log from the Näs locality showing section 2 (0 – 5.55m) and section 3 (0 – 0.6m)

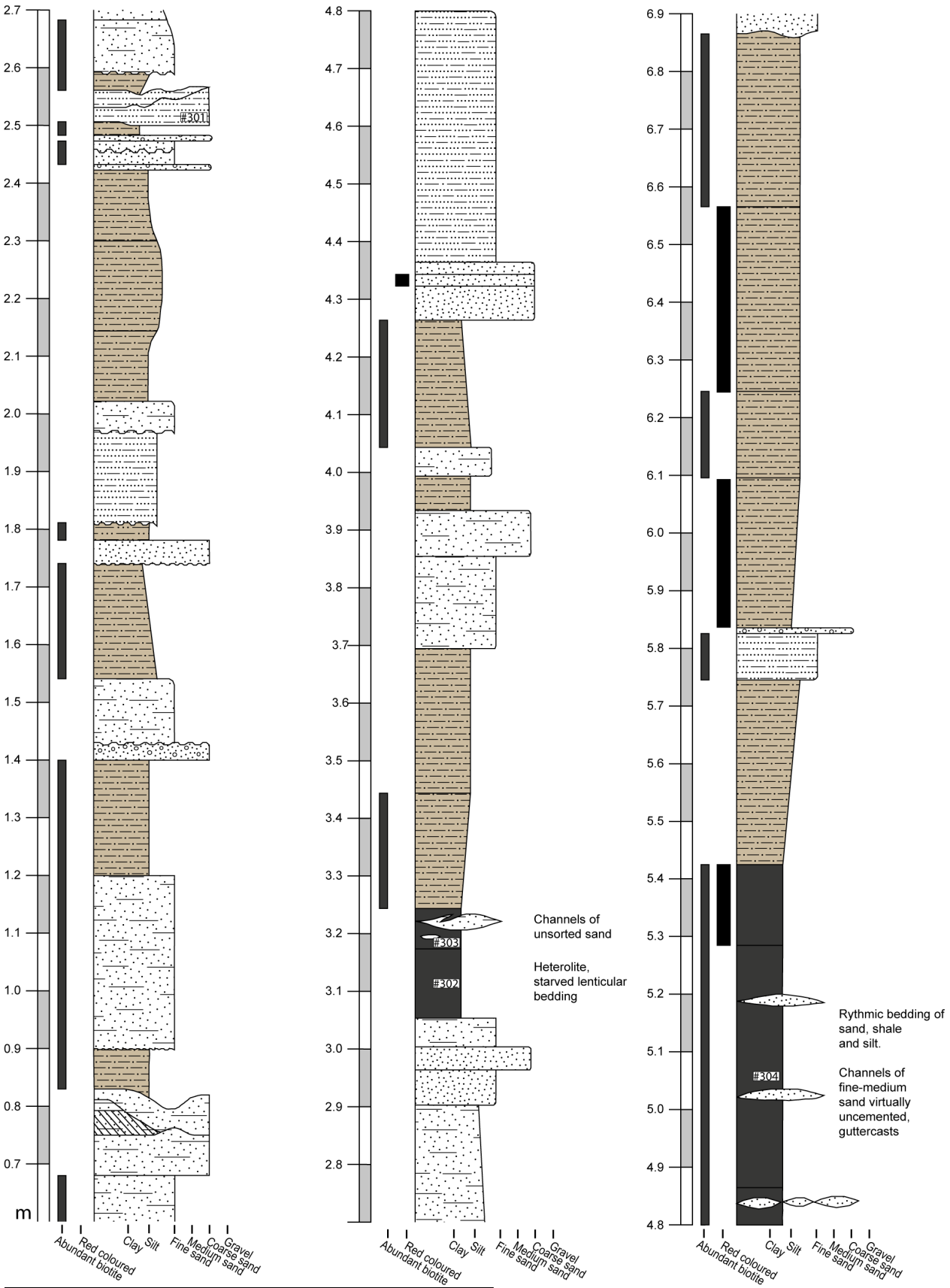

Figure 10. Stratigraphic log from the Näs locality showing section 3 (0.7 – 6.9m).

Figure 11. Stratigraphic log from the Näs locality showing section 3 (6.9 – 13.2m)

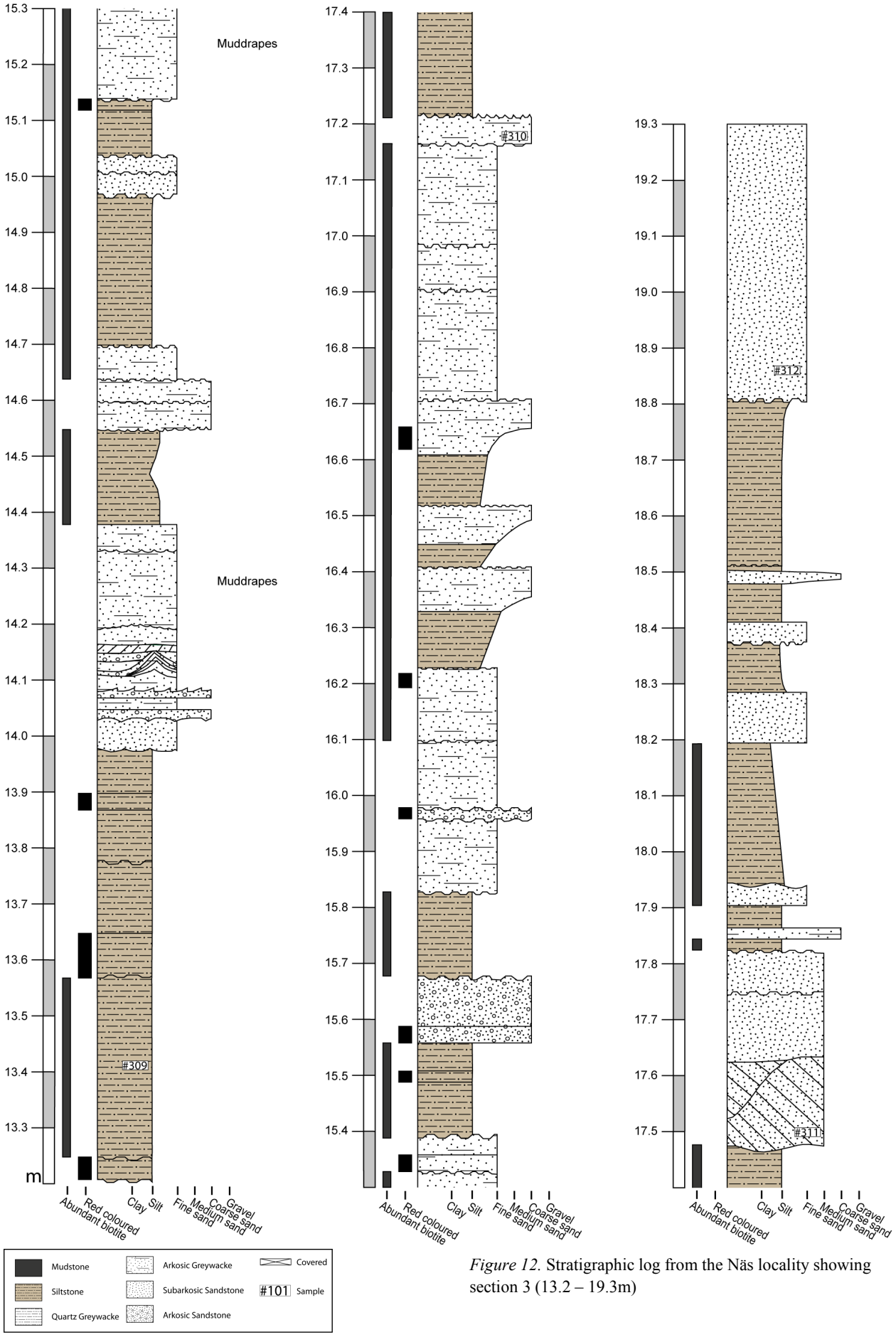

Figure 12. Stratigraphic log from the Näs locality showing section 3 (13.2 – 19.3m)

Ma. The most prominent peaks are 1.8, 1.7 and 1.48 Ga. A majority of the peaks falls within the span of 1.61 – 1.85 Ga. A majority of the zircons in sample 306 belong to the rounded morphology group; angular grains had ages of c. 1052 Ma, 1447 Ma and several grains in the interval 1722-1831 Ma.

Sample 308 have age-peaks at: 2.0 Ga, 1.92 Ga, 1.81 Ga, 1.76 Ga, 1.68 Ga, 1.65 Ga, 1.62 Ga, 1.53 Ga, 1.47 Ga, 1.35 Ga, 1.3 Ga, 1.25 Ga, 1.21 Ga and 1.04 Ga (Fig. 13). A weighted mean of the three youngest zircons equaled 1004 ± 10 (MSWD = 0.29, Probability of fit = 0.75). The major age peaks are 1.68, 1.65 and 1.62 Ga. The peaks span a majority of the age spectrum, two gaps occur at 1.04 - 1.21 Ga and c. 1.85 and 1.92 Ga. Sample 308 was dominated by rounded grains. Angular grains occurred in the interval 1086 - 1227 Ma, at 1531 Ma and 1760 – 1770 Ma interval.

Sample 312 contained age peaks at: 1.98 Ga, 1.8 Ga, 1.7 Ga, 1.59 Ga, 1.53 Ga, 1.47 Ga, 1.37 Ga, 1.34 Ga, 1.16 Ga and 0.99 Ga (Fig. 13). Similarily to sample 306, sample 312 only contained one zircon in its youngest group with an age of 997 ± 11 Ma and the next closest was 110 Ma older so no weighted mean was produced for this sample. Major age peaks occur

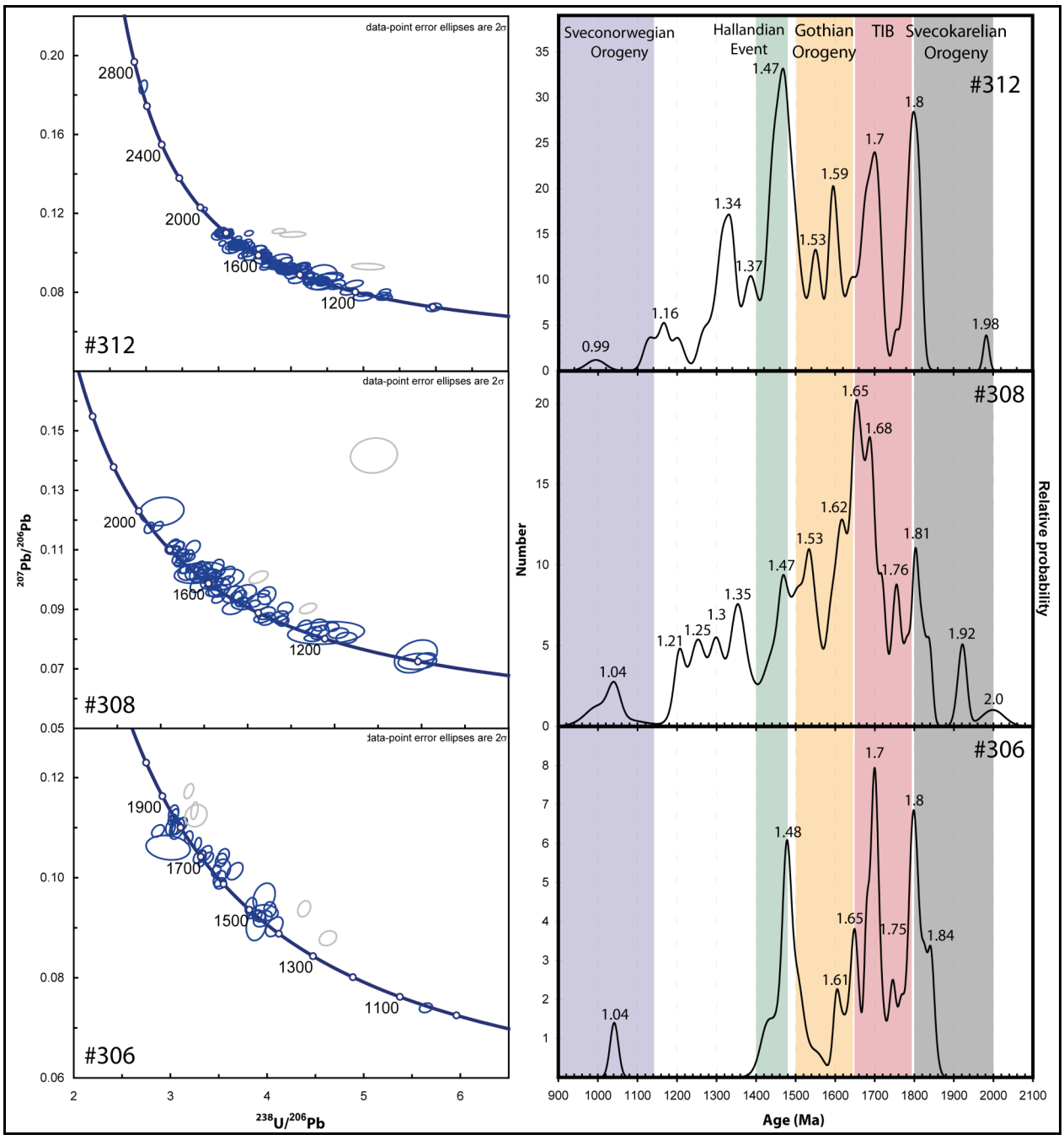

Figure 13. Tera-Wasserburg plots for samples 306, 308 and 312 (Rejected analyses marked in grey) and probability density plots of detrital zirons in stratigraphic order from the Näs locality. Coloured bars indicate timing of regional tectonic events.

at 1.8, 1.7, 1.59 and 1.47 Ga. Again the rounded grains dominated in sample 312 with individual angular grains occurring at 1364 Ma, 1417 Ma, 1430 Ma, 1462 Ma, 1494 Ma and 1550-1554 Ma. Several angular grains also occurred in the interval 1771-1851 Ma.

4.4 Detrital baddeleyite

In binocular microscope the grains appeared in various brown hues. In the Scanning Electron Microscope the tabular prismatic crystal habit were revealed in two of the grains (Fig. 14). All grains displayed irregular fractures, possibly caused during sorting and handpicking. The grains range in size from c. 50-60 μm on their a-axis. Detrital Baddeleyite have previously only been described from soils and rivers in proximity to igneous and metamorphic rocks, ferro-manganese nodules from the Indian Ocean and within the Triassic Smith Bank formation in the North Sea (Nayak et al. 2011; Wilkins et al. 2015).

5 Discussion

5.1 Lithology

The mudstone represents the most fine-grained facies of the studied interval. The small grain size and undisturbed lamination indicates an environment with very low energy levels and deposition through suspended material (Tucker 2009). Mudstones are normally diagnostic for shelf areas but the many sandy channels and lenses indicate a tidally influenced setting proximal to the shoreline (Martin 2000). Therefore the relative lack of coarser feldspar-rich material within the mudstones is likely caused by a starvation of sediment supply rather than the distance to the shoreline. The heterolithic textures indicate a setting with two dominating energy levels: One that is low enough to deposit mud, and one that is strong enough to deposit the sand fractions. Most often such deposition is inferred to be tidal which, based on the overall setting of the depositional basin, is very likely to be the case for the heterolithes of the investigated outcrops (cf. Collinson et al. 2006). Note however that heterolithes could also be produced in fluvial and glacial settings (Martin 2000) and the heterolithes of the Middle Formation was described by Larsen & Nørgaard-Pedersen (1988) as the result of wave-reworking of a predominantly mud based sediment provided with pulses of sandy material.

The Siltstone, Quartz Greywacke and Arkosic Greywacke facies have a similar depositional history with being deposited as mass flows and consisting of mixed lithologies. The unsorted composition of the facies points towards a fast mode of deposition as there is little to no evidence of hydrodynamic sorting (Tucker 2009). They are however problematic as they are generally displaying few sedimentary structures. Mass flows such as turbidites and sedimentary gravity flows will display Bouma-sequences, various forms of graded beds and water-escape structures (Bouma 1962; Middleton & Hampton 1973). Their massive structure also becomes a problem due to the fact if this should be interpreted as a sign of post-depositional alteration of the sediments or if it represents an original mode of deposition. Several studies have concluded that the matrix of the greywackes in the Middle Formation have been diagenetically formed (Morad & Al Dahan 1982; Morad 1983a; Morad 1984). However Larsen & Nørgaard-Pedersen (1988) pointed out that these studies have been done on medium to coarse -grained sandstones which does not conclude a diagenetic formation of the matrix in more fine-grained equivalents. Larsen & Nørgaard-Pedersen (1988) also stated that a part of the matrix was likely to represent primary phyllosilicate minerals as the closely related lithology of the various facies would not yield a varied matrix content if they initially had the same composition. Furthermore Larsen& Nørgaard-Pedersen (1988) argued that the massive structure with outsize clasts spread throughout the sediment indicates that the sediments had certain buoyancy at the time of deposition which would indicate primary clay-water content.

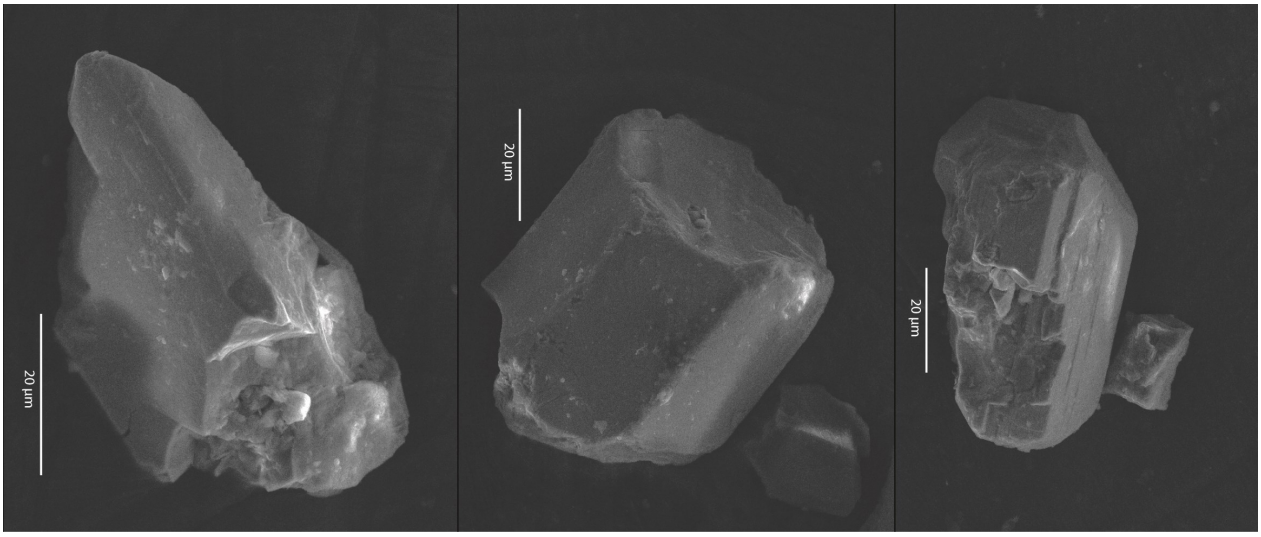

Figure 14. Backscattered electron images of detrital baddeleyite grains found within the samples from the Näs locality.

In this paper some Greywackes are labelled as such despite their sometimes higher than 75% clay content that would put them within the Mudstone bracket following conventional definitions (Tucker 2009). This is done because parts of the matrix was diagenetically formed and the original rocks likely had a lower clay-content, coupled with the mode of formation as instantaneous sediment-flows and their overall similarity to Greywackes containing less than 75% clay content.

Larsen & Nørgaard-Pedersen (1988) concluded that the sediments were deposited as sheet flows of coarse-grained sediments that continued as density flows, or subaqueous debris flows that integrated mud and water. They further strengthened their hypothesis by the fact that acritarchs had been subject to rapid burial within these sediments (Vidal 1976). Larsen & Nørgaard-Pedersen (1988) states that some beds require a different interpretation as they are more likely to have been deposited as fine-grained debris flows subject to weak reworking of wave-action and intermittent suspension deposition. The evidence they argue are the many desiccation cracks and discontinuity surfaces.

The views presented by Larsen & Nørgaard-Pedersen (1988) are supported in this paper. No evidence to discredit their interpretation has been found during the field work and their interpretation is consistent with the sequence stratigraphic framework for the formation (which is presented in chapter 5.2).

Siltstones requires very low energy levels in order for it to be deposited so the environment in which the siltstone settled must have been relatively calm. . Siltstones in general are often deposited in conjunction with deltas and close to the shoreline. Facies S is interpreted to represent the first stage of prograding delta lobes. An interval in section 3 between 11.3 – 11.9 m with plentiful ripples could possible represent proximity to a beach rather than a delta-lobe.

The Quartz Greywacke is interpreted as the next stage in a delta-lobe development as the environment becomes more proximal and sediment flows containing larger grain fractions are being deposited. The relatively low content of feldspars indicates that the source of the sediment is mainly from material transported further away and less is supplied from the vicinity of the basin.

The Arkose Geywacke is similar to the Quartz Greywacke but with high content of feldspars that indicates a bimodal sediment-source with the feldspars (especially the more angular) likely deriving from the vicinity of the rift margins. The varied composition and small amount of grain size sorting indicates a lack of processes that are able to sort the sediments. The deposition itself was probably quick in some form of sediment flow. Several dark laminae were observed in thin section (Fig. 6D). If these are of organic origin it could indicate that there were pauses in between depositional events that provided the organism with enough time to develop. Another possibility is that the laminae are thin mud drapes that could similarly represent pauses in which suspension deposition had time to cover the underlying sediments.

The Subarkosic Sandstone consistently displays hummocky cross-stratification (HCS). HCS is considered to be a constituent of tempestite deposits in the shoreface to off-shore transition zone (Harms 1975). However there is an ongoing debate regarding the actual origin of HCS and what hydrological process that forms it (Quin 2011). HCS and structures similar to HCS have been observed in a wide array of depositional environments from distal shelfs, lacustrine environments, intertidal flats, estuarine settings and within turbidites (Quin 2011). Nonetheless the HCS of the studied interval are likely generated through storm events as they also display laminated deposition and erosional surfaces in accord with idealized models for tempestites (Brenchley 1989).

Facies AS represents the episodic influx of immature sediment derived from the rift margins of the basin as feldspars as less likely to survive longer transport distances (Dickinson & Suczek 1979). The amount of arkosic sandstone seems to be tied to the proximity of the shoreline: the more proximal the setting, the more influx of arkosic sandstone. However the arkosic sandstone is incorporated in nearly all of the other facies to some degree. The deposition of thin homogenous layers that is dominated by feldspars could represent flows directly from talus cones into the basin. However the prevailing depositional setting is likely transport and depositon together with other sediments as some form of mass flow.

5.2 Sequence stratigraphy

The Visingsö Group, together with other Precambrian sediments, suffer from the lack of body- and ichnofossils as bathymetric indicators when making sequence stratigraphic analyses (Christie-Blick et al. 1995). Furthermore the few beds that contain carbonate in the Näs section have been affected by diagenetic alteration and thus another form of bathymetric indicator in the form of stable isotope data is unavailable. Left is process-sedimentology which is partly hindered by the relative uniform grain-size distribution and the uncertainty regarding how much diagenesis has altered the original sediment composition. All of these factors make it difficult to produce a sequence stratigraphical framework using conventional models as it becomes hard to identify typical sequences that define the various system tracts. Therefore the proposed sequence stratigraphic model for rift-basins, outlined in Martins-Neto & Catuneanu (2012), is used in this paper.

Tectonism is the major factor that creates new accommodation space within rift basins and a particular stratigraphic cyclicity develops within them (Martins-Neto & Catuneanu 2012). Accommodation space is created in short bursts of subsidence created by extension of the rift or fault reactivation. These short bursts are often followed by longer time periods

when tectonism is inactive and no new accommodation space is generated leading to sediments filling up the basin and consuming all available accommodation space (Martins-Neto & Catuneanu 2012). Rift basins are therefore dominated by coarsening upwards sequences representing progradational depositional trends that fill in the newly created accommodation space. This is in turn followed by a short retrogradational stage of a transgressive systems tract that develops due to the subsidence created by tectonic activity. After this the progradational pattern repeats itself and a complete cycle of sedimentation is completed when the next tectonic pulse and subsequent transgression occurs (Martins-Neto & Catuneanu 2012). This is a pattern that that happens on several hierarchical levels and several smaller sequences can often be discerned within larger ones. However a rift sequence can be disturbed by factors such as varying stretching rates of the rift during its evolution and fluctuations in sea-level due to climate (Martins-Neto & Catuneanu 2012).This type of repeated progradational patterns is present in the sections at Näs in the form of the many coarsening-upwards cycles terminating with bathymetrical indicators of very shallow conditions followed by deposition of deep marine mudstone (Fig. 15).

The sequence boundaries in rift successions are identified by the flooding surfaces created by the rapid creation of accommodation space during a tectonic event that results in a sudden transgression (Martins-Neto & Catuneanu 2012). Typically a sequence in a rift begins with deep water deposits on top of a flooded surface. These are lain down after rapid subsidence and the following transgression (Martins-Neto & Catuneanu 2012). Following this definition leads to the placement of the sequence boundaries for the Näs sections within the intervals of Mudstone Lithofacies. As seen in figure 7C the mudstones have a clear divide between heterolithic intervals and deep marine mudstone shale and they should arguably be treated as two distinct lithofacies contrary to this papers classification of only one Mudstone facies. The sequence boundaries are located at this divide where the deposition changes from a shallow tidally influenced setting to deep marine sedimentation representing the transgressive interval (Fig. 15).

The sediment supply often increases right after a tectonic event when the relief between source area and the basin changes (Martins-Neto & Catuneanu 2012). In some rift basins with limited accommodation space there is an initial sandy layer beneath the flooding surface that represents the onset of the rifting (Prosser 1993).

A rift basin has three depositional conditions: under-filled, filled and over-filled. The under-filled consists of turbidite facies within finer grained successions that follows the first flooding surfaces (Martins-Neto & Catuneanu 2012). This can be seen throughout the sections at Näs with the deposition of the siltstones and greywackes as mass flows with an analogous mode of deposition to the turbidites outlined in the model for rift basins. However this interpretation can not explain the occurances of desiccation cracks within these lithofacies. The filled stage of a rift basin encompasses an upwards pro-gradation to shallow-water and coastal systems (Martins-Neto & Catuneanu 2012) which again can be seen within the Näs sections as the coarsening-upwards cycles start displaying bathymetric indicators that points towards deposition over the FWWB. The overfilled space is, in this model, represented by alluvial sediments (Martins-Neto & Catuneanu 2012), whereas within the Näs section this stage is represented by the heterolithic mudstone and the sediments containing desiccation cracks rather than true alluvial sediments. A major difference between a rift sequence and a basin in a tectonically stable area is the asymmetrical base-level curve which is a function of the long periods of tectonic quiescence in between pulses of activity. This leads to an absence or poor development of the low stand system tract (Martins-Neto & Catuneanu 2012). A rift sequence is built up of transgressive systems tracts and high stand system tracts. The high stand systems tract is the major constituent of the sequence and in turn consists of the progradational coarsening-upward successions that follows the maximum flooding surface (Martins-Neto & Catuneanu 2012). The transgressive system tract is represented by the retrogradational facies that are formed by tectonic subsidence (Martins-Neto & Catuneanu 2012). Hence the vast majority of the sediments of the Näs sections belong to the high stand systems tracts with the mudstone that follows the heterolithic intervals representing the transgressive systems tract (Fig. 15). Flooding surfaces and sediments of the transgressive systems tracts are generally good marker beds for intra-basin correlations within rift-basins. The same holds true for the mudstones of the Näs sections. They represent a depositional setting on a basin-wide scale and their distinct lithologies compared to other sediments make them easy to identify. Overall the cyclicities and depositional trends are in accordance with the rift-basin model and a depositional environment largely controlled by tectonism. The trend of progradational – retrogradational cycles, the types of deposition through the various phases of infilling and the lithological composition fits with the rift-basin model. The cycles in the Näs sections are however terminated by tidal sediments instead of true alluvial sediments outlined in the model. The lack of sand layers beneath the flooding surfaces indicate sufficient accommodation space so is more likely that the sediment supply controlled the deposition. A possible scenario is that large tidal-flat areas developed in the overfilled basin as the sediment supply diminished.

5.3 Provenance

A tentative estimation of source areas for specific age intervals was produced (Fig. 16) by defining specific provenance regions that largely coincide with the lithotectonic units of southern Sweden. The prove-

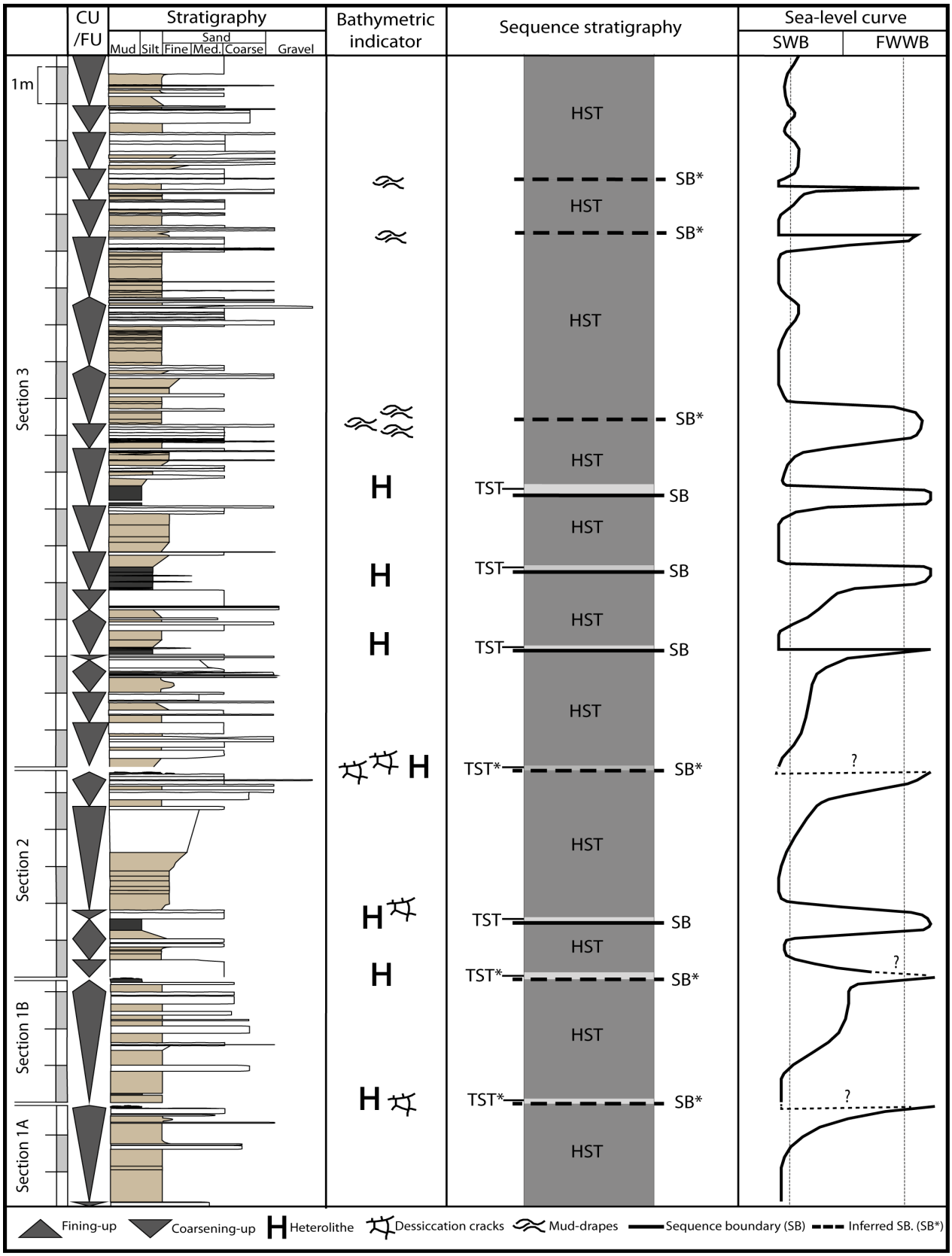

Figure 15. Proposed sequence stratigraphy and sea-level curve for the Näs sections. Coarsening up-wards trend (CU), fining up-wards trend (FU). Condensed stratigraphic log: Heterolithic Mudstone (Facies M. Dark grey), Siltstone (Facies S. Grey) and greywackes and sandstones (Facies: QGW, AGW, SST & AST. White). Bathymetric indicators found within the sections. Proposed sequence stratigraphic framework: HST = highstand systems tract, TST = transgressive systems tract, SB = sequence boundary. Asterisks indicate inferred occurrences. Proposed sea-level curve: SWB = Storm wave base, FWWB = fair-weather wave base.

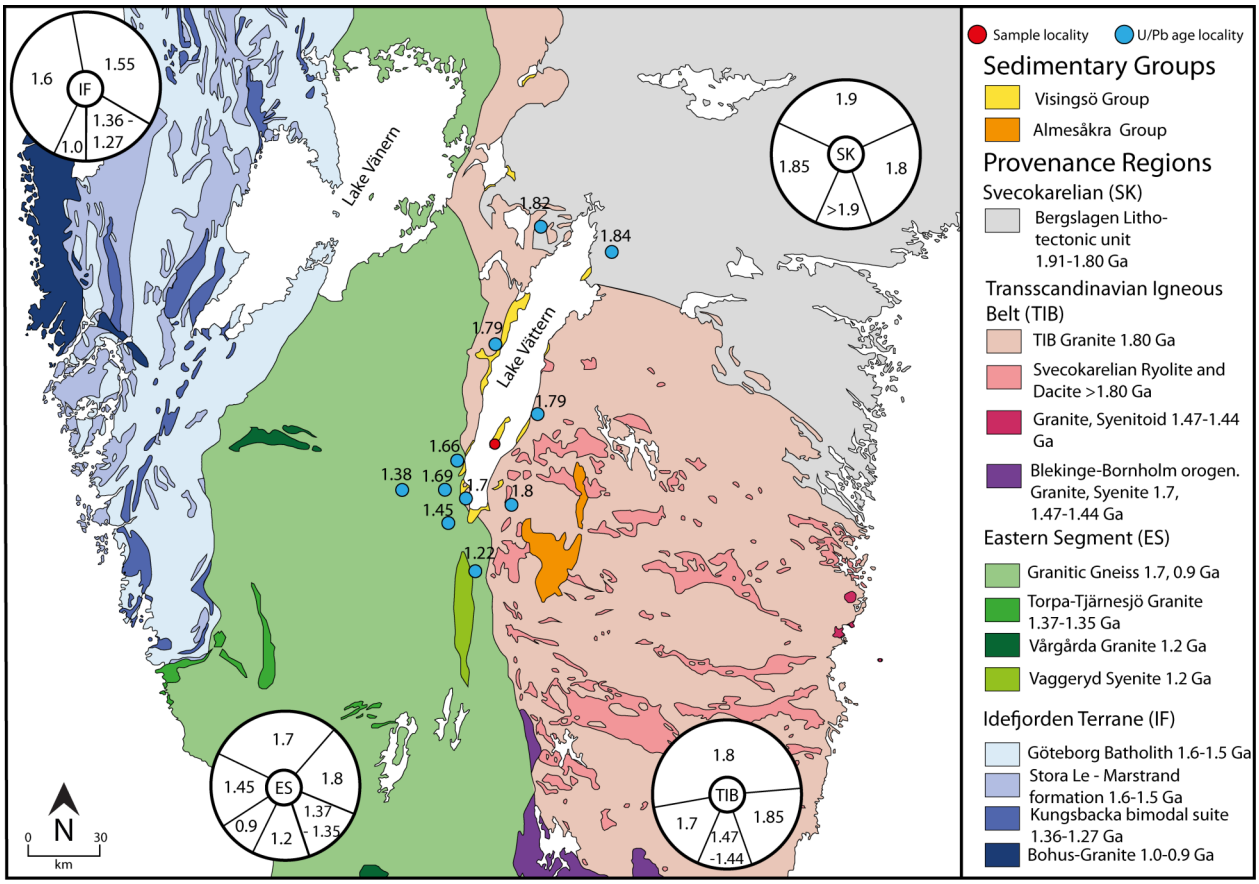

Figure 16. Map showing protolith ages for rocks in south-central Sweden. Red dot indicates sample locality for the data presented herein from the Näs sections at Visingsö. Blue dots are a selection of localities of dated Zircon in the vicinity of Lake Vättern. Pie-charts represent a tentative estimation of the proportion of rocks that belongs to specific ages based on their present day distribution. Based on maps, data and references in the Geochronological database provided by Swedish Geological Survey (© Sveriges Geologiska Undersökning).

nance regions were named: The IF region (Idefjorden), ES region (Eastern Segment), TIB region (Transcandinavian Igneous belt) and SK region (Svecokarelian) after the names commonly used to denote these areas. Furthermore ages were linked to specific rocks that could be the proto-source for the sediments using the ages of previous zircon U/Pb analyses conducted after the year 2000 within the mapped area (Table. 2)

The principles outlined in Vermeesch (2004) concludes that 117 grains should be dated in a provenance study. This provides a 95% confidence that an age-fraction compromising more than 5% of the total amount has not been missed. Due to loss of zircon grains during preparation and analyses the three samples yielded varying amounts of U/Pb dates. Sample 306, 308 and 312 supplied 42, 82 and 127 measurements respectively. In effect only sample 312 contains enough for a robust provenance assessment and caution should be taken not to draw conclusions on missing age groups within samples 306 and 308.

Furthermore before any discussion can be done regarding the provenance of the sediments one has to take into account that the present day distribution of rocks likely differs from the distribution in the Neoproterozoic. Subduction occurred on the present day western side of Southern Sweden and rocks were displaced towards the east. The present day boundary for how far the ductile deformation of the Sveconorwegian Orogeny affected the bedrock is the Sveconorwegian Front. However the Almesåkra Group (Fig. 16) contains evidence that the effects of the orogeny spanned even further east and crustal nappes likely covered parts of the area (Rodhe 1987; Möller & Andersson 2018). This could for instance make the interpretation of the IF region ages as a more far-travelled westerly component incorrect as nappes consisting of these rocks might very well have existed much farther to the east.

The age assemblage in sample 306 (Fig. 17) contains age peaks that can be traced to rocks in close proximity to the present day Vättern Basin (Fig. 16). Noteworthy is the complete lack of zircons in the span between 1.04 - 1.48 Ga. That these ages are missing could indicate a very close source for the zircons as trocks with these ages are generally found further away than the ones that are present in sample 306. However any interpretation of missing age peaks with-

Table 2. Age peaks discerned through: relative probability diagrams from the Näs sections, which regions within the mapped area in figure 16 where U/Pb analyses of zircon have confirmed these ages and references to the specific analyses.

Age peaks (Ga)	Location of analysis	References
2.0, 1.98 & 1.92	SK region	(Andersson et al. 2006; Johansson & Stephens 2017)
1.84	North-eastern TIB region, southern SK region	(Söderlund et al. 1999; Åhäll & Larson 2000; Wikström & Persson 2002; Kleinhanns et al. 2015)
1.81–1.80	North-eastern & central TIB region, vicinity of Lake Vättern	(Andreasson et al. 1987; Appelquist et al. 2008; Eliasson et al. 2008; Appelquist et al. 2009; Kleinhanns et al. 2015; Petersson et al. 2015; Petersson et al. 2017)
1.76-1.75	Southern TIB region	(Nilsson & Wikman 1997; Johansson et al. 2006)
1.7-1.68	South-western, central, south-eastern ES region, vicinity of Lake Vättern	(Scherstén et al. 2000; Söderlund et al. 2002; Brander et al. 2012; Petersson et al. 2017)
1.65	Vicinity of Lake Vättern, Western IF region	(Appelquist et al. 2008; Brander et al. 2012) (Petersson et al. 2015)
1.62, 1.61 & 1.59	Northern & central IF region	(Scherstén et al. 2004; Ahlin et al. 2006; Åhäll & Connelly 2008; Austin Hegardt 2010; Petersson et al. 2015)
1.53	Central IF region	(Åhäll & Connelly 2008; Austin Hegardt 2010)
1.48–1.47	Southern & eastern TIB region, Eastern ES region & vicinity of Lake Vättern	(Åhäll 2001; Söderlund & Ask 2006; Brander & Söderlund 2009)
1.37, 1.35–1.34	Southern & western ES region, vicinity of Lake Vättern	(Andersson et al. 1999; Brander et al. 2012; Möller et al. 2015; Petersson et al. 2015)
1.3	Central IF region	(Hegardt et al. 2007; Söderlund et al. 2008)
1.25	Northern IF region	(Persson et al. 1983)
1.21	Vicinity of Lake Vättern, central & eastern ES region	(Åhäll & Connelly 1998; Söderlund & Ask 2006)
1.16		
1.04	Southern & central IF region	(Hegardt et al. 2007; Söderlund et al. 2008)
0.99	Western & southern ES region	(Wang et al. 1998; Möller et al. 2015)

in sample 306 becomes speculative due to insufficient amount of analyses. Furthermore the missing ages are present in sample 308, 312 and all three samples from the Lower- and Middle formations of the Visingsö Group shown in the study by Moczydłowska et al. (2017). With the missing age peaks being prevalent throughout other parts of the Visingsö Group it is unlikely that they should be missing throughout the Näs sections, especially as the 1.04 and 1.61 Ga age peaks indicates that far travelled components could reach the basin. It is therefore likely that their absence is due to insufficient data.

Sample 308 (Fig. 17) contains the most diverse age assemblage of the three samples, it contains all of the various ages found in the vicinity of the basin together with the Svecokarelian peaks 2.0 and 1.92 Ga and the distinctively western IF region peak 1.53 Ga. The IF- and SK region components suggest that sample 308 has an influx of sediments that have undergone transport before being deposited. Sample 312 (Fig. 17) has the same dominant peaks as sample 306 (1.8, 1.7 and 1.47 Ga) coupled with a Svecokarelian component as well as distinctively IF region age peaks at 1.59 and 1.54 Ga. The age peak 1.16 Ga does not occur within the mapped area of figure 16, however this age can be linked to bimodal plutonism and volcanism

that occurred between 1169 – 1134 Ma in the Telemarkia Terrane (Bingen & Solli 2009) in southern Norway (Northwest of the mapped area in Fig 16).

Sample 306 consists of a Quartz Greywacke which has been interpreted herein to be derived of material that has been transported some distance before being deposited because of the relatively few feldspar grains that it contains. However the age assemblage points to a local source area as the ages fits with many rocks in the vicinity of Lake Vättern. The same pattern can be discerned within sample 312 that consists of a Subarkosic Sandstone where a large part is derived in the immediate vicinity with a few minor, presumably, far travelled components. Sample 308 is the most fine grained and most diverse in terms of age peaks. Whilst many of the ages in sample 308 are still from the vicinity of Lake Vättern the ages have a more even distribution with less pronounced local peaks and overall there are more ages that could hail from the IF region.

A possible explanation why the most fine-grained sample holds the most diverse assemblage of zircon ages might be discerned with the sequence stratigraphic interpretations provided in this paper. The heterolithic mudstone of sample 308 is thought to have been deposited during a time of tectonic quiescence; this is in contrast to sample 306 and 312 that are thought to be deposited in the aftermath of tectonic activity that increased the amount of locally derived sediments through active displacement of material and increased the relief to surrounding areas and thus creating more material available for erosion. This influx of local sediments could produce the distinct age peaks within sample 306 and 312. Sample 308 in turn is likely to contain more material that has been transported further distances. However whilst an increase in amount of locally derived sediments could produce the distinct age peaks the amount of zircon in the sediments could also be due to various sampling biases such as: the rocks inherently containing different amount of zircon, failure to produce a representative selection during the hand picking of zircons or that certain age groups produced too small or poor quality zircons that could not be analysed.

The presented age distributions (Fig. 17) are in accord with the cumulative probability diagrams created with rock samples from the easternmost parts of Sveconorwegian orogeny and the Sveconorwegian front (Bingen & Solli 2009). The presented age groups published in Moczydłowska et al. (2017) from a 'quartz-arkosic sandstone' of the Middle Formation from the island of Visingsö are similar to the ones presented herein but do not contain the pronounced peaks at 1.8 and 1.7 Ga found within the samples 306 and 312. Instead their age distribution resembles the herein inferred tectonically calm sample 308. This could be

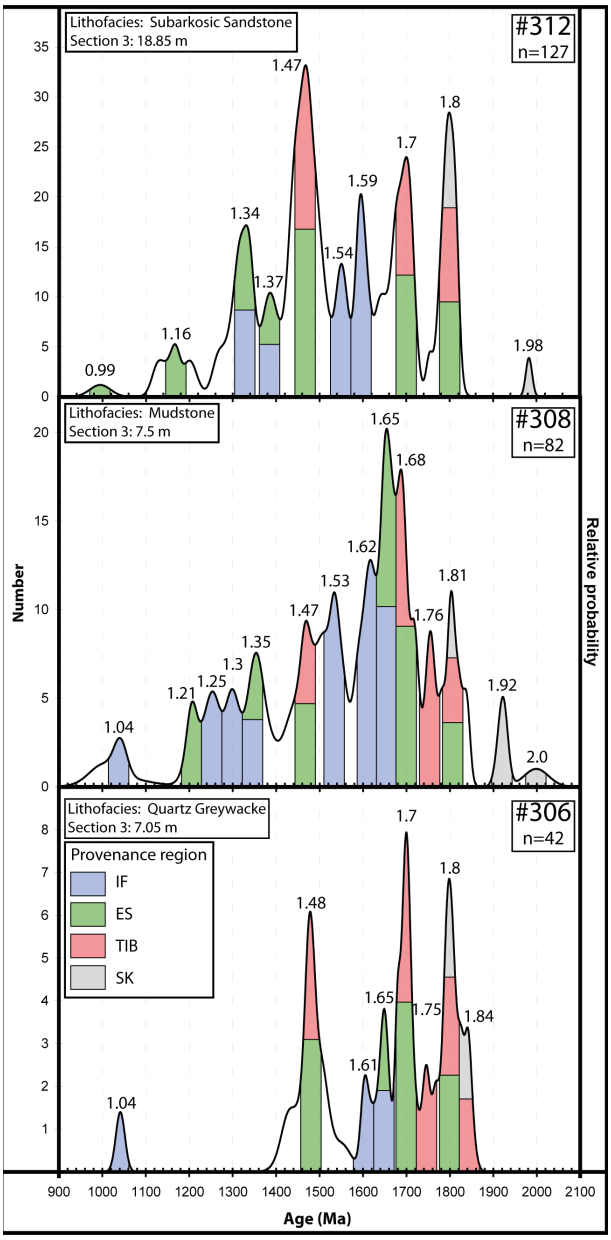

Figure 17. Visualization of possible source areas for detrital zircon from the Näs locality using relative probability diagrams presented elsewhere in this paper. Coloured bars indicate possible provenance regions that could have yielded these ages (Data presented elsewhere in this paper). Coloured bars does not indicate amounts of zircons.

due to a varying influx of sediments to different areas of the basin, or the sediments were deposited at different times with varied tectonic activity. A possibility exist that the difference could be due to large areas of TIB-aged rocks were covered by younger sediments and hence more zircons with younger ages were predominantly being eroded. But since the stratigraphical relationship between the localities is unknown it becomes speculative.

Moczydłowska et al. (2017) concluded that the minimum depositional age increased the further up in the stratigraphy they investigated (The lower for-

mation having a minimum depositional age of c. 886 Ma increasing to c 990 and 1045 Ma in the Middle Formation). This pattern cannot be discerned within the samples from the Näs assemblage (which only contains samples from the Middle Formation). Sample 306 has a youngest zircon age of 1041 ± 21 Ma, progressing into 1000 ± 62 in sample 308, and 994 ± 48 in sample 312. However only sample 308 provided a group of young zircons so that a mean average could be produced. This average of 1004 ± 10 Ma is similar to the ages presented in the Middle Formation samples of Moczydłowska et al. (2017) and provide a rough estimate of c. 990 – 1004 Ma as a minimum depositional age for the Middle Formation of the Visingsö Group.

The morphology of the zircon assemblages from the Näs outcrops points to a varied origin of its sediments. The rounded shapes indicate that a large part of the assemblage have gone through metamorphism and/or transport (Corfu et al. 2003). The more angular grains points to magmatic, and possibly volcanic, origins (Corfu et al. 2003). The fact that angular grains seems to represent certain ages in the data presented herein, most notably the c. 1750-1850 Ma range, is likely a result of a short transport distance that would preserve original features. Rocks of these ages are present in the immediate surrounding of the present day basin (Fig. 16). The well preserved crystal structures in grains indicate a consistently calm geologic environment throughout the burial of the sediments, however, a local event, such as the hydrothermal alterations that was reported by Ödman (1942) from the Visingsö Group, could be obscured due to the low stratigraphic resolution of the zircon samples.

Overall the three samples contain a large portion of zircons that derive from rocks that can be found in the Lake Vättern area today. A smaller component of material with a source of further transported material that is indicated to derive from IF- and ES region sources and a small number from the north-eastern SK region. This view is consistent with previous sedimentological interpretations that determined that the sediments are of a bimodal composition with a locally derived feldspar-rich and a further travelled quartz rich component (Vidal 1976; Larsen & Nørgaard-Pedersen 1988). That a large part of the zircons stem from the TIB, ES and IF regions is consistent with palaeocurrent evidence suggesting a general flow towards the northeast (Larsen & Nørgaard-Pedersen 1988). However due to the insufficient amount of analyses it becomes highly speculative to draw conclusions about how different aged rocks were distributed at the time of deposition.

6 Conclusions

- 6 distinct lithofacies were identified within the Näs sections. The sediments are defined by: immature mineralogy and composition, a short transport distance and evidence of a wave-influenced depositional setting. The deposition of the Subarkosic Sandstones within the studied outcrops is mainly related to storm events evident by sedimentary structures such as the hummocky cross-stratification.
- Parts of the sediment have undergone very little transport evident by the presence of detrital baddeleyite, prismatic zircons, and the abundance of feldspar.
- The sedimentary cycles and depositional trends of the Näs outcrops are largely in accord with existing rift-basin models. The sequence stratigraphical framework points to a sediment-supply that is driven by tectonic activity. A tectonic event creates new accommodation space and a transgressive episode occurs as the mudstones of the transgressive systems tract are deposited. The under filled basin is filled in by the deposition of coarsening-upwards cycles that corresponds to the highstand systems tract until tectonic quiescence and an overfilled basin limits the available space and sediment supply. Thus enabling deposition of the heterolithic mudstones. The cycle is then repeated with the next tectonic event.
- The provenance of the sediments indicates that they are largely derived from rocks in the relative vicinity of the basin, again indicating a short transport before deposition. The ages are in accordance with previous studies from the Middle Formation in other parts of the basin, as well as for cumulative probability diagrams generated for this area.
- The age groups are present throughout the region and can be tied to Svecokarelian rocks (2.0 –1.75 Ga), the Transscandinavian igneous belt (c. 1.86–1.66 Ga), the Gothian orogeny (1.66–1.52 Ga), Hallandian event (1.47–1.38 Ga), the Eastern Segment- and Idefjorden regions (1.21-1.37 Ga) the Telemarkia Terrane (1.16 Ga) and the Sveconorwegian orogeny (1.14–0.90 Ga).
- The sequence stratigraphical framework and geochronological data hints at a tectonically driven shift of sediment-supply to the basin: A background-sedimentation consisting of a mix of local and further transported sediments during calm episodes and an increase of local sediments from the vicinity of the basin during periods of tectonic activity.

7 Acknowledgements

Thanks go out to my supervisor Mikael Calner for his support, guidance and overall enthusiasm with the project. Also for allowing me the amount of freedom and independence that I have enjoyed which have taught me many valuable lessons as I've been finding my way through this project.

Tomas Næraa, Ulf Söderlund and Anna Sartell are thanked for taking time out of their schedules and spare time in order to help me with analyses and guiding me through the field of geochronology.

Other huge thanks go out to Anders Lindskog, Mats Eriksson and Per Ahlberg for their open door policies, the many varied discussions and their overall enthusiasm.

Agneta Månsson Klausen is thanked for discussions on the Vättern Basin and for providing that one elusive article that tied this entire thesis together.

Friends and family are thanked for their continued support and finally; further thanks go to fellow students in Periklas on the 5th floor for their invaluable help and providing much needed social interaction throughout the late evenings and weekends. Special thanks go out to Johan Solanum Tuberosum, Josefine Martelle and Christopher Robin 'Veitsi' Jansson.

8 References

Åhäll, K.-I., 2001: *Åldersbestämning av svårdaterade bergarter i sydöstra Sverige*. SKB**.**

Åhäll, K.-I. & Connelly, J., 1998: Intermittent 1.53–1.13 Ga magmatism in western Baltica; age constraints and correlations within a postulated supercontinent. *Precambrian Research 92***,** 1-20.

Åhäll, K.-I. & Connelly, J. N., 2008: Long-term convergence along SW Fennoscandia: 330 my of Proterozoic crustal growth. *Precambrian Research 161***,** 452-474.

Åhäll, K.-I. & Larson, S. Å., 2000: Growth-related 1.85–1.55 Ga magmatism in the Baltic Shield; a review addressing the tectonic characteristics of Svecofennian, TIB 1-related, and Gothian events. *GFF 122***,** 193-206.

Ahlin, S., Hegardt, E. A. & Cornell, D., 2006: Nature and stratigraphic position of the 1614 Ma Delsjön augen granite-gneiss in the Median Segment of south-west Sweden. *GFF 128***,** 21-32.

Allen, J., 1981: Lower Cretaceous tides revealed by cross-bedding with mud drapes. *Nature 289***,** 579.

Andersson, J., Söderlund, U., Cornell, D., Johansson, L. & Möller, C., 1999: Sveconorwegian (-Grenvillian) deformation, metamorphism and leucosome formation in SW Sweden, SW Baltic Shield: constraints from a Mesoproterozoic granite intrusion. *Precambrian Research 98***,** 151-171.

Andersson, U. B., Högdahl, K., Sjöström, H. & Bergman, S., 2006: Multistage growth and reworking of the Palaeoproterozoic crust in the Bergslagen area, southern Sweden: evidence from U–Pb geochronology. *Geological Magazine 143***,** 679-697.

Andréasson, P.-G. & Rodhe, A., 1990: Geology of the Protogine Zone south of Lake Vättern, southern Sweden: a reinterpretation. *Geologiska Föreningen i Stockholm Förhandlingar 112***,** 107-125.

Andreasson, P.-G., Solyom, Z. & Johansson, I., 1987: Geotectonic significance of Mn-Fe-Ba and Pb-Zn-Cu-Ag mineralizations along the Sveconorwegian-Grenvillian front in Scandinavia. *Economic Geology 82***,** 201-207.

Andréasson, P. & Dallmeyer, R., 1995: Tectonothermal evolution of high□alumina rocks within the Protogine Zone, southern Sweden. *Journal of Metamorphic Geology 13***,** 461-474.

Appelquist, K., Cornell, D. & Brander, L., 2008: Age, tectonic setting and petrogenesis of the Habo Volcanic Suite: Evidence for an active continental margin setting for the Transscandinavian Igneous Belt. *GFF 130***,** 123-138.

Appelquist, K., Eliasson, T., Bergström, U. & Rimša, A., 2009: The Palaeoproterozoic Malmbäck Formation in S Sweden: age, composition and tectonic setting. *GFF 131***,** 229-243.

Arnaud, E., Halverson, G. P. & Shields-Zhou, G., 2011: The geological record of Neoproterozoic ice ages. *Geological Society, London, Memoirs 36***,** 1-16.

Arthur Holmes, A., 1911: The association of lead with uranium in rock-minerals, and its application to the measurement of geological time. *Proc. R. Soc. Lond. A 85***,** 248-256.

Austin Hegardt, E., 2010: *Pressure, temperature and time constraints on tectonic models for southwestern Sweden*. Department of Earth Sciences; Institutionen för geovetenskaper**.**

Axberg, S. & Wadstein, P., 1980: *Distribution of the sedimentary bedrock in Lake Vättern, southern Sweden*. Almqvist & Wiksell international (distr.)**.**

Barrell, J., 1917: Rhythms and the measurements of geologic time. *Bulletin of the Geological Society of America 28***,** 745-904.

Berg, W., 1872: Visingsö som konungasäte. *Svenska Fornminnesföreningens Tidsskrift 3***,** 261-272.

Bingen, B., Belousova, E. & Griffin, W., 2011: Neoproterozoic recycling of the Sveconorwegian orogenic belt: Detrital-zircon data from the Sparagmite basins in the Scandinavian Caledonides. *Precambrian Research 189***,** 347-367.

Bingen, B., Nordgulen, Ø. & Viola, G., 2008: A four-phase model for the Sveconorwegian orogeny, SW Scandinavia. *Norwegian Journal of Geology/Norsk Geologisk Forening 88*.

Bingen, B. & Solli, A., 2009: Geochronology of magmatism in the Caledonian and Sveconorwegian belts of Baltica: synopsis for detrital zircon provenance studies. *Norwegian Journal of Geology/Norsk Geologisk Forening 89*.

Bogdanova, S., 2001: Tectonic settings of 1.65–1.4 Ga AMCG magmatism in the western East European Craton (western Baltica). *Journal of Conference Abstracts.* 769 pp.

Bogdanova, S., Bingen, B., Gorbatschev, R., Kheraskova, T., Kozlov, V., Puchkov, V. & Volozh, Y. A., 2008: The East European Craton (Baltica) before and during the assembly of Rodinia. *Precambrian Research 160***,** 23-45.

Bonhomme, M. G. & Welin, E., 1983: Rb—Sr and K—Ar isotopic data on shale and siltstone from the Visingsö group, Lake Vättern basin, Sweden. *Geologiska Föreningen i Stockholm Förhandlingar 105***,** 363-366.

Bouma, A. H., 1962: Sedimentology of some flysch deposits. *Agraphic approach to facies interpretation 168*.

Brander, L., Appelquist, K., Cornell, D. & Andersson, U. B., 2012: Igneous and metamorphic geochronologic evolution of granitoids in the central Eastern Segment, southern Sweden. *International Geology Review 54***,** 509-546.

Brander, L. & Söderlund, U., 2009: Mesoproterozoic (1.47–1.44 Ga) orogenic magmatism in Fennoscandia; Baddeleyite U–Pb dating of a suite of massif-type anorthosite in S. Sweden. *International journal of earth sciences 98***,** 499-516.

Brenchley, P. J., 1989: Storm sedimentation. *Geology Today 5***,** 133-137.

Brewer, T., Åhäll, K.-I., Menuge, J., Storey, C. & Parrish, R., 2004: Mesoproterozoic bimodal volcanism in SW Norway, evidence for recurring pre-Sveconorwegian continental margin tectonism. *Precambrian Research 134***,** 249-273.

Brocks, J., Jarrett, A., Sirantoine, E., Kenig, F., Moczydłowska, M., Porter, S. & Hope, J., 2016: Early sponges and toxic protists: possible sources of cryostane, an age diagnostic biomarker antedating Sturtian Snowball Earth. *Geobiology 14***,** 129-149.

Brotzen, F., 1941: Några bidrag till visingsöformationens stratigrafi och tektonik. *Geologiska Föreningen i Stockholm Förhandlingar 63***,** 245-261.

Butterfield, N. J., 2015: The neoproterozoic. *Current Biology 25***,** R859-R863.

Cawood, P. A. & Hawkesworth, C. J., 2014: Earth's middle age. *Geology 42***,** 503-506.

Cawood, P. A. & Pisarevsky, S. A., 2006: Was Baltica right-way-up or upside-down in the Neoproterozoic? *Journal of the Geological Society 163***,** 753-759.

Cawood, P. A. & Pisarevsky, S. A., 2017: Laurentia-Baltica-Amazonia relations during Rodinia assembly. *Precambrian Research 292***,** 386-397.

Christie-Blick, N., Dyson, I. A. & Von Der Borch, C., 1995: Sequence stratigraphy and the interpretation of Neoproterozoic Earth history. *Precambrian Research 73***,** 3-26.

Coint, N., Slagstad, T., Roberts, N., Marker, M., Røhr, T. & Sørensen, B. E., 2015: The Late Mesoproterozoic Sirdal Magmatic Belt, SW Norway: relationships between magmatism and metamorphism and implications for Sveconorwegian orogenesis. *Precambrian Research 265***,** 57-77.

Collini, B. 1951: Visingsöformationen. *In* P. Geijer, B. Collini & H. Munthe (eds.): *Beskrivning till kartbladet Gränna.*, 22-36. Sveriges Geologiska Undersökning,

Collinson, J., Mountney, N. & Thompson, D., 2006: *Sedimentary structures*. Terra Publishing, Harpenden, England**.**

Corfu, F., Hanchar, J. M., Hoskin, P. W. & Kinny, P., 2003: Atlas of zircon textures. *Reviews in Mineralogy and Geochemistry 53***,** 469-500.

Corte, A. & Higashi, A., 1964. Experimental research on desiccation cracks in soil. COLD REGIONS RESEARCH AND ENGINEERING LAB HANOVER NH Report.

Dickinson, W. R. & Suczek, C. A., 1979: Plate tectonics and sandstone compositions. *Aapg Bulletin 63***,** 2164-2182.

Egerton, R. F., 2005: *Physical principles of electron microscopy*. Springer**.**

Eliasson, T., Persson, P. & Bergström, U., 2008: U–Pb zircon age of a TIB-1 quartz monzonite from Hultseryd north-east of Jönköping, south central Sweden. *Results from radiometric datings and other isotope analyses 2***,** 8-10.

Ewetz, C., 1932: Fossilrester i Visingsöformationen. *Geologiska Föreningen i Stockholm Förhandlingar 54***,** 310-314.

Ewetz, C., 1933: Einige neue Fossilfunde in der Visingsöformation. *Geologiska Föreningen i Stockholm Förhandlingar 55***,** 506-518.

Gaál, G. & Gorbatschev, R., 1987: An outline of the Precambrian evolution of the Baltic Shield. *Precambrian Research 35***,** 15-52.

Gee, D. G. & Stephenson, R. A., 2006: The European lithosphere: an introduction. *Geological Society, London, Memoirs 32***,** 1-9.

Gehrels, G., 2014: Detrital zircon U-Pb geochronology applied to tectonics. *Annual Review of Earth and Planetary Sciences 42***,** 127-149.

Gorbatschev, R. & Bogdanova, S., 1993: Frontiers in the Baltic shield. *Precambrian Research 64***,** 3-21.

Gower, C., Ryan, A. & Rivers, T., 1990: Mid-Proterozoic Laurentia–Baltica: an overview of its geological evolution and a summary of the contributions made by this volume. *Mid-Proterozoic Laurentia-Baltica 38***,** 1-20.

Halverson, G. P., Wade, B. P., Hurtgen, M. T. & Barovich, K. M., 2010: Neoproterozoic chemostratigraphy. *Precambrian Research 182*, 337-350.

Harland, W. B. & Rudwick, M. J., 1964: The great infra-Cambrian ice age. *Scientific American 211*, 28-37.

Harms, J. C., 1975: Depositional environments as interpreted from primary sedimentary structures and stratification sequences. *Soc Econ Paleont Miner Short Course 2*, 161p.

Hayes, J. M., Strauss, H. & Kaufman, A. J., 1999: The abundance of 13C in marine organic matter and isotopic fractionation in the global biogeochemical cycle of carbon during the past 800 Ma. *Chemical Geology 161*, 103-125.

Hegardt, E. A., Cornell, D. H., Hellström, F. A. & Lundqvist, I., 2007: Emplacement ages of the mid-Proterozoic Kungsbacka bimodal suite, SW Sweden. *GFF 129*, 227-234.

Hiess, J., Condon, D. J., Mclean, N. & Noble, S. R., 2012: 238U/235U systematics in terrestrial uranium-bearing minerals. *Science 335*, 1610-1614.

Hoffman, P. F., 1991: Did the breakout of Laurentia turn Gondwanaland inside-out? *Science 252*, 1409-1412.

Hoffman, P. F., Kaufman, A. J., Halverson, G. P. & Schrag, D. P., 1998: A Neoproterozoic snowball earth. *Science 281*, 1342-1346.

Högdahl, K., Andersson, U. B. & Eklund, O., 2004: *The Transscandinavian Igneous Belt (TIB) in Sweden: a review of its character and evolution*. Geological survey of Finland Espoo.

Holm, E. J. G., 1885: *Om Vettern och Visingsöformationen*.

Holmes, A. & Lawson, R. W., 1927: Factors involved in the calculation of radioactive minerals. *American Journal of Science*, 327-344.

Horodyski, R. J., 1993: Paleontology of Proterozoic shales and mudstones: examples from the Belt Supergroup, Chuar Group and Pahrump Group, western USA. *Precambrian Research 61*, 241-278.

Hubbard, F. H., 1975: The Precambrian crystalline complex of south-western Sweden. The geology and petrogenetic development of the Varberg Region. *Geologiska Föreningen i Stockholm Förhandlingar 97*, 223-236.

Jackson, S. E., Pearson, N. J., Griffin, W. L. & Belousova, E. A., 2004: The application of laser ablation-inductively coupled plasma-mass spectrometry to in situ U–Pb zircon geochronology. *Chemical Geology 211*, 47-69.

Johansson, Å., Bogdanova, S. & Čečys, A., 2006: A revised geochronology for the Blekinge Province, southern Sweden. *GFF 128*, 287-302.

Johansson, Å. & Stephens, M. B., 2017: Timing of magmatism and migmatization in the 2.0–1.8 Ga accretionary Svecokarelian orogen, south-central Sweden. *International journal of earth sciences 106*, 783-810.

Karlstrom, K. E., Åhäll, K.-I., Harlan, S. S., Williams, M. L., Mclelland, J. & Geissman, J. W., 2001: Long-lived (1.8–1.0 Ga) convergent orogen in southern Laurentia, its extensions to Australia and Baltica, and implications for refining Rodinia. *Precambrian Research 111*, 5-30.

Kirschvink, J. L., 1992: Late Proterozoic low-latitude global glaciation: the snowball Earth.

Kleinhanns, I., Whitehouse, M. J., Nolte, N., Baero, W., Wilsky, F., Hansen, B. & Schoenberg, R., 2015: Mode and timing of granitoid magmatism in the Västervik area (SE Sweden, Baltic Shield): Sr–Nd isotope and SIMS U–Pb age constraints. *Lithos 212*, 321-337.

Knoll, A. H. & Vidal, G., 1980: Late Proterozoic vase-shaped microfossils from the Visingsö Beds, Sweden. *Geologiska Föreningen i Stockholm Förhandlingar 102*, 207-211.

Kumpulainen, R. & Nystuen, J., 1985: Late Proterozoic basin evolution and sedimentation in the westernmost part of Baltoscandia. *The Caledonide Orogen—Scandinavia and Related Areas 1*, 213-245.

Larsen, B. T., Olaussen, S., Sundvoll, B. & Heeremans, M., 2008: The Permo-Carboniferous Oslo Rift through six stages and 65 million years. *Episodes 31*, 52-58.

Larsen, M. & Nørgaard-Pedersen, N., 1988: A sedimentological analysis of deltaic complexes and alluvial fan deposits in the Visingsö Group (Upper Proterozoic), Southern Sweden. *Institut for Almen Geologi Københavns Universitet*.

Li, Z.-X., Bogdanova, S., Collins, A., Davidson, A., De Waele, B., Ernst, R., Fitzsimons, I., Fuck, R., Gladkochub, D. & Jacobs, J., 2008: Assembly, configuration, and break-up history of Rodinia: a synthesis. *Precambrian Research 160*, 179-210.

Lind, G., 1972: The gravity and geology of the Vättern area, southern Sweden. *Geologiska Föreningen i Stockholm Förhandlingar 94*, 245-257.

Linnarsson, G., 1880a: De äldsta paleozoiska lagren i trakten kring Motala. *Geologiska Föreningen i Stockholm Förhandlingar 5*, 23-30.

Linnarsson, G., 1880b: Om de geologiska förhållandena i trakten kring Hjo. *Geologiska Föreningen i Stockholm Förhandlingar 5*, 102-108.

Loron, C. & Moczydłowska, M., 2017: Tonian (Neoproterozoic) eukaryotic and prokaryotic organic-walled microfossils from the upper Visingsö Group, Sweden. *Palynology*, 1-35.

Lundmark, A. M. & Lamminen, J., 2016: The provenance and setting of the Mesoproterozoic Dala Sandstone, western Sweden, and paleogeographic implications for southwestern

Fennoscandia. *Precambrian Research 275*, 197-208.
Magnusson, N. H., 1960: Age determinations of Swedish Precambrian rocks. *Geologiska Föreningen i Stockholm Förhandlingar 82*, 407-432.
Maloof, A. C., Schrag, D. P., Crowley, J. L. & Bowring, S. A., 2005: An expanded record of Early Cambrian carbon cycling from the Anti -Atlas Margin, Morocco. *Canadian Journal of Earth Sciences 42*, 2195-2216.
Martin, A., 2000: Flaser and wavy bedding in ephemeral streams: a modern and an ancient example. *Sedimentary Geology 136*, 1-5.
Martin, H., 1939: *Die Post-Archäische Tektonik im südlichen Mittelschweden;(Mit Taf. IV u. 41 Abb. im Text u. auf 8 Textbeil.)*. Schweizerbart.
Martins-Neto, M. & Catuneanu, O. 2012: Rift sequence stratigraphy. *In Regional Geology and Tectonics: Phanerozoic Rift Systems and Sedimentary Basins*, 58-70. Elsevier,
Merdith, A. S., Collins, A. S., Williams, S. E., Pisarevsky, S., Foden, J. D., Archibald, D. B., Blades, M. L., Alessio, B. L., Armistead, S. & Plavsa, D., 2017: A full-plate global reconstruction of the Neoproterozoic. *Gondwana Research 50*, 84-134.
Middleton, G. V. & Hampton, M. A., 1973: Part I. Sediment gravity flows: mechanics of flow and deposition.
Moczydłowska, M., Pease, V., Willman, S., Wickström, L. & Agić, H., 2017: A Tonian age for the Visingsö Group in Sweden constrained by detrital zircon dating and biochronology: Implications for evolutionary events. *Geological Magazine*, 1-15.
Möller, C. & Andersson, J., 2018: Metamorphic zoning and behaviour of an underthrusting continental plate. *Journal of Metamorphic Geology*.
Möller, C., Andersson, J., Dyck, B. & Lundin, I. A., 2015: Exhumation of an eclogite terrane as a hot migmatitic nappe, Sveconorwegian orogen. *Lithos 226*, 147-168.
Morad, S., 1983a: Diagenesis and geochemistry of the Visingso Group (Upper Proterozoic), Southern Sweden: a clue to the origin of color differentiation. *Journal of Sedimentary Research 53*.
Morad, S., 1983b: *Petrology of the Visingsö Group (upper Proterozoic), Southern Sweden*. University of Uppsala. Institute of Geology. Department of Mineralogy and Petrology.
Morad, S., 1984: Diagenetic matrix in Proterozoic graywackes from Sweden. *Journal of Sedimentary Research 54*.
Morad, S. & Al Dahan, A. A., 1982: *Mineralogy and crystal-chemistry of clay minerals related to diagenesis and very low-grade metamorphism of two Proterozoic sedimentary sequences from Sweden*. University of Uppsala, Institute of Geology.
Munthe, H. & Gavelin, A. O., 1907: *Beskrifning till kartbladet Jönköping*. Kungl. boktryckeriet, PA Norstedt & söner.
Mus, M. M. & Moczydlowska, M., 2000: Internal morphology and taphonomic history of the Neoproterozoic vase-shaped microfossils from the Visings Group, Sweden. *Norsk Geologisk Tidsskrift 80*, 213-228.
Nagy, R. M., Porter, S. M., Dehler, C. M. & Shen, Y., 2009: Biotic turnover driven by eutrophication before the Sturtian low-latitude glaciation. *Nature Geoscience 2*, 415.
Nasdala, L., Zhang, M., Kempe, U., Panczer, G., Gaft, M., Andrut, M. & PlöTze, M., 2003: Spectroscopic methods applied to zircon. *Reviews in Mineralogy and Geochemistry 53*, 427-467.
Nathorst, A., 1879a: En egendomlig strukturvarietet af lerhaltig kalksten från Grennatrakten. *Geologiska Föreningen i Stockholm Förhandlingar 4*, 213-217.
Nathorst, A. G., 1879b: Om de åldre sandstens-och skifferbildningarne vid Vettern. *Geologiska Föreningen i Stockholm Förhandlingar 4*, 421-436.
Nathorst, A. G., 1886: Några ord om Visingsöserien. *Geologiska Föreningen i Stockholm Förhandlingar 8*, 5-23.
Nathorst, A. G. & Kramer, J. H., 1884: *Upplysningar till geologisk öfversigtskarta öfver Sverige: södra bladet; skala 1: 1.000. 000*. Sveriges Geologiska Undersökning.
Nayak, B., Das, S. K. & Bhattacharyya, K. K., 2011: Detrital and authigenic (?) baddeleyite (ZrO2) in ferromanganese nodules of Central Indian Ocean Basin. *Geoscience Frontiers 2*, 571-576.
Nilsson, M. & Wikman, H., 1997: U-Pb zircon ages of two Småland dyke porphyries at Påskallavik and Alsterbro, southeastern Sweden. *Radiometric dating results 3*, 31-40.
Norrman, J. O., 1964: Lake Vättern: investigations on shore and bottom morphology. *Geografiska Annaler 46*, 1-238.
Ödman, O. H. R., 1942: *Copper Ores of the"red Beds" Type from Visingsö, Sweden*. Kungl. boktryckeriet, PA Norstedt & söner.
Ogg, J. G., Ogg, G. & Gradstein, F. M., 2016: *A concise geologic time scale: 2016*. Elsevier.
Page, L. M., Möller, C. & Johansson, L., 1996: 40Ar39Ar geochronology across the Mylonite Zone and the Southwestern Granulite Province in the Sveconorwegian Orogen of S Sweden. *Precambrian Research 79*, 239-259.
Patchett, P. J., 1978: *Rb/Sr ages of Precambrian dolerites and syenites in southern and central Sweden*. Sveriges geologiska undersökning.

Paton, C., Hellstrom, J., Paul, B., Woodhead, J. & Hergt, J., 2011: Iolite: Freeware for the visualisation and processing of mass spectrometric data. *Journal of Analytical Atomic Spectrometry 26*, 2508-2518.

Paton, C., Woodhead, J. D., Hellstrom, J. C., Hergt, J. M., Greig, A. & Maas, R., 2010: Improved laser ablation U□Pb zircon geochronology through robust downhole fractionation correction. *Geochemistry, Geophysics, Geosystems 11*.

Persson, L., Bruun, Å. & Vidal, G., 1985: *Beskrivning till berggrundskartan Hjo SO*. Sveriges Geologiska Undersögning.

Persson, P.-O., Wahlgren, C.-H. & Hansen, B. T., 1983: U-Pb ages of Proterozoic metaplutonics in the gneiss complex of southern Värmland, south-western Sweden. *Geologiska Föreningen i Stockholm Förhandlingar 105*, 1-8.

Petersson, A., Bjärnborg, K., Scherstén, A., Gerdes, A. & Næraa, T., 2017: Tracing Proterozoic arc mantle Hf isotope depletion of southern Fennoscandia through coupled zircon U–Pb and Lu–Hf isotopes. *Lithos 284*, 122-131.

Petersson, A., Scherstén, A., Bingen, B., Gerdes, A. & Whitehouse, M. J., 2015: Mesoproterozoic continental growth: U–Pb–Hf–O zircon record in the Idefjorden terrane, Sveconorwegian orogen. *Precambrian Research 261*, 75-95.

Porter, S. M. 2006: The Proterozoic fossil record of heterotrophic eukaryotes. *In Neoproterozoic geobiology and paleobiology*, 1-21. Springer,

Porter, S. M. & Knoll, A. H., 2000: Testate amoebae in the Neoproterozoic Era: evidence from vase-shaped microfossils in the Chuar Group, Grand Canyon. *Paleobiology 26*, 360-385.

Prosser, S., 1993: Rift-related linked depositional systems and their seismic expression. *Geological Society, London, Special Publications 71*, 35-66.

Quin, J. G., 2011: Is most hummocky cross□stratification formed by large□scale ripples? *Sedimentology 58*, 1414-1433.

Rino, S., Kon, Y., Sato, W., Maruyama, S., Santosh, M. & Zhao, D., 2008: The Grenvillian and Pan-African orogens: world's largest orogenies through geologic time, and their implications on the origin of superplume. *Gondwana Research 14*, 51-72.

Rodhe, A., 1987: *Depositional environments and lithostratigraphy of the Middle Proterozoic Almesåkra Group, southern Sweden*. Sveriges geologiska undersökning.

Rogers, J. J. & Santosh, M., 2002: Configuration of Columbia, a Mesoproterozoic supercontinent. *Gondwana Research 5*, 5-22.

Rosén, S., 1925: Konglomeratens vittnesbörd om Visingsöformationens geologiska ålder. *Geol. Foren. Stockh. Forh 47*, 365-366.

Scherstén, A., Årebäck, H., Cornell, D., Hoskin, P., Åberg, A. & Armstrong, R., 2000: Dating mafic–ultramafic intrusions by ion-microprobing contact-melt zircon: examples from SW Sweden. *Contributions to Mineralogy and Petrology 139*, 115-125.

Scherstén, A., Larson, S. Å., Cornell, D. & Stigh, J., 2004: Ion probe dating of a migmatite in SW Sweden: the fate of zircon in crustal processes. *Precambrian Research 130*, 251-266.

Schoene, B., 2014: 4.10-U–Th–Pb Geochronology. *Treatise on geochemistry 4*, 341-378.

Shields-Zhou, G., Hill, A. & Macgabhann, B. 2012: The Cryogenian Period. *In The geologic time scale*, 393-411. Elsevier,

Sircombe, K. N. & Stern, R. A., 2002: An investigation of artificial biasing in detrital zircon U-Pb geochronology due to magnetic separation in sample preparation. *Geochimica et Cosmochimica Acta 66*, 2379-2397.

Söderlund, U. & Ask, R., 2006: Mesoproterozoic bimodal magmatism along the Protogine Zone, S Sweden: three magmatic pulses at 1.56, 1.22 and 1.205 Ga, and regional implications. *GFF 128*, 303-310.

Söderlund, U., Hellström, F. & Kamo, S., 2008: Geochronology of high□pressure mafic granulite dykes in SW Sweden: tracking the P–T–t path of metamorphism using Hf isotopes in zircon and baddeleyite. *Journal of Metamorphic Geology 26*, 539-560.

Söderlund, U., Isachsen, C. E., Bylund, G., Heaman, L. M., Patchett, P. J., Vervoort, J. D. & Andersson, U. B., 2005: U–Pb baddeleyite ages and Hf, Nd isotope chemistry constraining repeated mafic magmatism in the Fennoscandian Shield from 1.6 to 0.9 Ga. *Contributions to Mineralogy and Petrology 150*, 174.

Söderlund, U., Jarl, L.-G., Persson, P.-O., Stephens, M. B. & Wahlgren, C.-H., 1999: Protolith ages and timing of deformation in the eastern, marginal part of the Sveconorwegian orogen, southwestern Sweden. *Precambrian Research 94*, 29-48.

Söderlund, U. & Johansson, L., 2002: A simple way to extract baddeleyite (ZrO2). *Geochemistry, Geophysics, Geosystems 3*.

Söderlund, U., Möller, C., Andersson, J., Johansson, L. & Whitehouse, M., 2002: Zircon geochronology in polymetamorphic gneisses in the Sveconorwegian orogen, SW Sweden: ion microprobe evidence for 1.46–1.42 and 0.98–0.96 Ga reworking. *Precambrian Research 113*, 193-225.

Sonnenfeld, P., 1984: *Brines and evaporites*. Orlando; Toronto: Academic Press.

Strauss, J. V., Rooney, A. D., Macdonald, F. A., Brandon, A. D. & Knoll, A. H., 2014: 740 Ma vase-shaped microfossils from Yukon, Cana-

da: Implications for Neoproterozoic chronology and biostratigraphy. *Geology 42*, 659-662.
Talyzina, N. M., 2000: Ultrastructure and morphology of Chuaria circularis (Walcott, 1899) Vidal and Ford (1985) from the Neoproterozoic Visingsö Group, Sweden. *Precambrian Research 102*, 123-134.
Timofeev, B. V., 1960: Sur la caractéristique micropaléontologique de la formation de Visingsö. *Geologiska Föreningen i Stockholm Förhandlingar 82*, 28-42.
Torsvik, T., Smethurst, M., Meert, J. G., Van Der Voo, R., Mckerrow, W., Brasier, M., Sturt, B. & Walderhaug, H., 1996: Continental break-up and collision in the Neoproterozoic and Palaeozoic—a tale of Baltica and Laurentia. *Earth-Science Reviews 40*, 229-258.
Tucker, M. E., 2009: *Sedimentary petrology: an introduction to the origin of sedimentary rocks*. John Wiley & Sons.
Vermeesch, P., 2004: How many grains are needed for a provenance study? *Earth and Planetary Science Letters 224*, 441-451.
Vidal, G., 1972: Algal stromatolites from the Late Precambrian of Sweden. *Lethaia 5*, 353-367.
Vidal, G., 1974: Late Precambrian microfossils from the basal sandstone unit of the Visingsö beds, South Sweden. *Geologica et Palaeontologica 8*, 1-14.
Vidal, G., 1976: *Late Precambrian microfossils from the Visingso Beds in southern Sweden*. Universitetsforlaget.
Vidal, G., 1985: Prepaleozoisk sedimentberggrund. *Persson L, Bruun A, Vidal G, editors. Beskrivning till Berggrundskartan Hjo SO. Sveriges Geol Undersokning Serie Af 134*, 77-91.
Vidal, G. & Bylund, G., 1981: Late Precambrian boulder beds in the Visingsö Beds, south Sweden. *Earth's Pre-Pleistocene Glacial Record*, 629-631.
Vidal, G. & Ford, T. D., 1985: Microbiotas from the late Proterozoic Chuar Group (northern Arizona) and Uinta Mountain Group (Utah) and their chronostratigraphic implications. *Precambrian Research 28*, 349-389.
Vidal, G. & Moczydłowska-Vidal, M., 1997: Biodiversity, speciation, and extinction trends of Proterozoic and Cambrian phytoplankton. *Paleobiology 23*, 230-246.
Vidal, G. & Moczydłowska, M., 1995: The Neoproterozoic of Baltica—stratigraphy, palaeobiology and general geological evolution. *Precambrian Research 73*, 197-216.
Wahlgren, C.-H., Cruden, A. R. & Stephens, M. B., 1994: Kinematics of a major fan-like structure in the eastern part of the Sveconorwegian orogen, Baltic Shield, south-central Sweden. *Precambrian Research 70*, 67-91.
Wang, X.-D., Söderlund, U., Lindh, A. & Johansson, L., 1998: U–Pb and Sm–Nd dating of high-pressure granulite-and upper amphibolite facies rocks from SW Sweden. *Precambrian Research 92*, 319-339.
Wetherill, G. W., 1956: Discordant uranium□lead ages, I. *Eos, Transactions American Geophysical Union 37*, 320-326.
Wiedenbeck, M., Alle, P., Corfu, F., Griffin, W., Meier, M., Oberli, F. V., Quadt, A. V., Roddick, J. & Spiegel, W., 1995: Three natural zircon standards for U□Th□Pb, Lu□Hf, trace element and REE analyses. *Geostandards newsletter 19*, 1-23.
Wikström, A. & Persson, P.-O., 2002: A ca. 1845 Ma ("Askersund") age of the Hälla augen gneiss in south-eastern Osterg ötland, south-east Sweden. *Radiometric dating results 5*, 58-61.
Wilkins, A., Wilson, M., Morton, A., Hurst, A. & Archer, S., 2015: First recorded occurrence of detrital baddeleyite (ZrO2) in sedimentary rock (Smith Bank Formation, Triassic, Central North Sea). Geological Society of London.
Zenzén, N., 1925: Geologiska kartor och geologisk kartläggning i Sverige före upprättandet av Sveriges Geologiska Undersökning. *Geologiska Föreningen i Stockholm Förhandlingar 47*, 311-343

Appendix

I. Geochronological data

Table 3. LA-ICP-MS data for analyzed zircons from sample 306.

Spot	Morphology	U (ppm)	Th (ppm)	238U/206Pb	±σ	207Pb/206Pb	±σ	Conc. %	207Pb/206Pb (Ma)	±σ
L306-9	Pyramidal	221.1	192.7	5.643	0.054	0.0740	0.0008	101	1041	21
S306-6	Ovoid	154.8	275	4.630	0.073	0.0879	0.0012	91	1380	26
L306-28		308	92.3	4.075	0.073	0.0902	0.0016	99	1430	34
L306-11	Oblong	143	125.1	3.888	0.085	0.0905	0.0025	103	1436	53
L306-32	Oblong	205.1	117.7	3.956	0.078	0.0918	0.0013	99	1463	27
L306-48	Oblong	159.6	210.9	3.937	0.040	0.0922	0.0009	99	1472	18
L306-34	Oblong	288	633	3.897	0.039	0.0925	0.0008	100	1477	17
L306-5	Oblong	144.9	123.4	3.837	0.035	0.0929	0.0008	101	1485	17
L306-33	Pyramidal	551	274	3.975	0.114	0.0930	0.0013	97	1488	26
S306-2		110.2	87	4.031	0.050	0.0937	0.0012	95	1502	24
S306-16	Circular	117.1	107.3	4.384	0.054	0.0938	0.0013	88	1504	26
L306-45	Oblong	225.5	290	3.833	0.048	0.0943	0.0014	99	1514	28
S306-18		48.3	107.9	3.970	0.093	0.0961	0.0023	93	1550	45
S306-5	Oblong	426	403.1	3.515	0.049	0.0989	0.0009	101	1603	17
L306-26	Ovoid	215	211	3.509	0.053	0.0998	0.0013	100	1620	24
L306-24	Oblong	233	158	3.668	0.067	0.1013	0.0014	94	1648	26
S306-17	Circular	269.7	285	3.473	0.039	0.1013	0.0010	99	1649	17
L306-39	Ovoid	185	116.5	3.530	0.075	0.1016	0.0017	97	1654	31
L306-10	Oblong	281	243.4	3.320	0.026	0.1030	0.0007	101	1679	12
S306-15	Oblong	330	215	3.525	0.047	0.1035	0.0011	95	1688	20
S306-1		355	348	3.390	0.045	0.1039	0.0009	98	1696	17
L306-8	Oblong	666.6	592	3.300	0.051	0.1042	0.0011	100	1700	19
L306-38	Oblong	367	421	3.336	0.028	0.1043	0.0009	99	1702	15
S306-13	Ovoid	262.8	322	3.549	0.049	0.1043	0.0012	94	1702	21
L306-42	Oblong	632	302	3.360	0.056	0.1048	0.0013	98	1711	23
L306-47	Circular	166	112.2	2.976	0.186	0.1060	0.0020	108	1732	35
L306-12	Ovoid	169.8	173.9	3.286	0.027	0.1068	0.0009	98	1746	16
L306-35	Oblong	224	195	3.191	0.035	0.1081	0.0010	99	1768	17
L306-25	Oblong	728	519	2.872	0.053	0.1093	0.0010	108	1788	16
L306-4	Ovoid	471.3	402.7	3.067	0.062	0.1098	0.0017	101	1796	28
L306-3	Prismatic	279.9	142.4	3.068	0.043	0.1099	0.0010	101	1798	17
L306-30		238.8	218	3.000	0.040	0.1100	0.0012	103	1799	20
L306-15	Oblong	103.4	81	3.044	0.038	0.1103	0.0014	101	1804	23
L306-14	Prismatic	328	224	3.123	0.041	0.1107	0.0011	99	1811	18
L306-31		364	317	3.020	0.036	0.1116	0.0009	101	1826	14
S306-10	Prismatic	301.3	268	3.265	0.093	0.1124	0.0018	94	1839	29
L306-36	Prismatic	233.5	117	3.044	0.032	0.1126	0.0010	99	1841	15
L306-6	Oblong	147.2	122.2	3.033	0.042	0.1128	0.0014	100	1845	22
L306-41		183.9	194	3.249	0.030	0.1134	0.0014	93	1855	22
L306-20	Prismatic	241	278	3.191	0.041	0.1173	0.0012	92	1915	18

Table 4. LA-ICP-MS data for analyzed zircons from sample 308.

Spot	Morphology	U (ppm)	Th (ppm)	238U/206Pb	±σ	207Pb/206Pb	±σ	Conc. %	207Pb/206Pb (Ma)	±σ
S308-11	Ovoid	53.8	0.634	5.952	0.181	0.0725	0.002	100	1000	62
L308-32	Ovoid	303	6.6	6.050	0.088	0.0740	0.001	95	1041	30
S308-47	Circular	22.9	2.31	5.935	0.201	0.0742	0.005	96	1047	##
S308-54	Ovoid	399	153.5	4.748	0.079	0.0804	0.001	102	1206	22
L308-51	Ovoid	90	56.1	5.136	0.098	0.0804	0.002	95	1207	37
L308-39	Ovoid	232	163	5.045	0.092	0.0820	0.001	94	1246	33
S308-24	Prismatic	135	77.1	4.902	0.360	0.0821	0.003	96	1248	74
S308-9	Ovoid	136.3	409	4.831	0.084	0.0823	0.002	97	1253	45
L308-18	Prismatic	199	335	4.771	0.066	0.0826	0.001	97	1260	31
L308-11		134.9	77.6	4.968	0.067	0.0841	0.001	91	1295	28
L308-13	Oblong	184.7	445	4.658	0.063	0.0845	0.002	96	1304	34
S308-25		60.3	72.1	4.826	0.077	0.0847	0.002	93	1309	37
S308-48		72.9	25.07	4.403	0.056	0.0861	0.001	98	1340	31
S308-44		285.7	116	4.386	0.058	0.0864	0.001	98	1347	27
L308-21	Oblong	144.8	83.3	4.221	0.078	0.0868	0.002	101	1356	38
L308-6	Circular	1072	288.5	4.168	0.078	0.0870	0.001	102	1360	27
L308-25		124.2	170	4.361	0.086	0.0876	0.002	97	1374	33
S308-8	Oblong	225	181.5	4.211	0.087	0.0887	0.002	98	1398	37
S308-14	Ovoid	230	67	4.695	0.079	0.0903	0.001	87	1432	30
L308-12	Ovoid	117	139.9	4.433	0.071	0.0904	0.002	91	1434	34
L308-30		354.7	275	3.828	0.097	0.0904	0.002	104	1434	36
L308-2_2	Oblong	234.3	14.2	3.926	0.089	0.0914	0.001	101	1455	25
L308-46	Oblong	174	155.4	4.078	0.053	0.0919	0.001	96	1466	19
S308-46	Oblong	116.3	152.1	4.120	0.117	0.0924	0.002	95	1476	47
L308-23		304	248.5	3.931	0.057	0.0925	0.001	99	1478	27
S308-35		459	108.7	3.935	0.059	0.0926	0.001	99	1480	25
L308-24		418.2	252	3.660	0.058	0.0936	0.001	104	1500	24
L308-26	Oblong	100.1	88.7	3.867	0.057	0.0941	0.002	98	1510	30
L308-17	Ovoid	373	483	3.912	0.060	0.0946	0.002	97	1520	30
S308-40	Oblong	73.6	206	4.221	0.084	0.0946	0.002	90	1520	48
S308-5	Oblong	104.1	250	3.834	0.106	0.0950	0.002	98	1528	46
S308-10	Oblong	158.2	225.5	3.960	0.114	0.0952	0.003	95	1532	49
S308-22	Oblong	217.1	484	4.182	0.054	0.0953	0.001	90	1534	18
L308-9	Oblong	439	120	3.610	0.073	0.0960	0.001	102	1548	25
S308-38	Ovoid	313.2	241	3.664	0.094	0.0961	0.002	100	1550	31
S308-49	Ovoid	91.7	70.6	3.689	0.093	0.0975	0.002	98	1577	46
S308-1	Circular	231.5	323	3.626	0.058	0.0981	0.001	99	1588	21
L308-2_1	Oblong	192.7	122.1	3.434	0.077	0.0984	0.002	103	1594	42
S308-6		134.7	210	3.593	0.049	0.0990	0.001	99	1605	24
L308-40	Oblong	198.8	196	3.550	0.073	0.0991	0.002	100	1607	34
L308-3	Ovoid	401.4	272	3.635	0.070	0.0994	0.001	97	1613	21
L308-44	Ovoid	433	409	3.771	0.060	0.0997	0.001	94	1618	22
S308-39	Prismatic	175	234	3.731	0.181	0.1000	0.003	94	1624	54
S308-41	Circular	172.4	160.9	3.515	0.044	0.1002	0.001	99	1628	20
S308-13	Circular	144.1	100.1	3.608	0.057	0.1008	0.002	96	1639	28
S308-30		167	92	4.125	0.088	0.1008	0.002	85	1639	31
L308-15	Ovoid	214	264	3.490	0.043	0.1013	0.001	99	1648	20
L308-10	Ovoid	596	255.8	3.592	0.044	0.1013	0.001	96	1648	18
L308-33	Circular	228	184	3.448	0.051	0.1017	0.001	99	1655	22
S308-37	Oblong	151.3	201	3.421	0.071	0.1017	0.002	100	1655	38

Table 4 continued. LA-ICP-MS data for analyzed zircons from sample 308.

Spot	Morphology	U (ppm)	Th (ppm)	238U/206Pb	±σ	207Pb/206Pb	±σ	Conc. %	207Pb/206Pb (Ma)	±σ
L308-41	Circular	194.9	273.1	3.577	0.049	0.1018	0.001	96	1657	24
L308-22	Ovoid	347	281	3.766	0.071	0.1022	0.002	91	1664	33
L308-35		313	185	3.596	0.085	0.1023	0.001	95	1666	20
L308-37	Ovoid	81	17.2	3.448	0.238	0.1023	0.003	99	1666	52
S308-51	Ovoid	341	276	3.406	0.100	0.1024	0.002	99	1668	38
S308-42		183.9	251	3.317	0.096	0.1025	0.002	102	1670	40
L308-38	Oblong	172.5	249	3.482	0.057	0.1026	0.002	97	1672	29
L308-4	Circular	215.2	230.9	3.274	0.041	0.1034	0.001	102	1686	20
L308-27	Ovoid	417	327	3.275	0.056	0.1036	0.001	102	1690	21
L308-36	Circular	215	220	3.511	0.052	0.1036	0.001	96	1690	25
L308-28	Oblong	274	235	3.343	0.042	0.1037	0.001	100	1691	20
L308-7	Ovoid	238	145.7	3.427	0.042	0.1041	0.001	97	1698	21
S308-23	Ovoid	89.1	126.2	3.659	0.055	0.1047	0.002	91	1709	30
L308-1	Oblong	516	405	3.455	0.039	0.1051	0.001	95	1716	15
L308-47	Oblong	350	507	3.202	0.034	0.1055	0.001	102	1724	17
S308-53	Oblong	321.7	263.7	3.211	0.064	0.1069	0.002	100	1747	29
L308-48		390	397	3.252	0.061	0.1072	0.001	99	1752	22
S308-16		366	473	3.324	0.056	0.1074	0.001	97	1756	19
S308-29	Oblong	258.5	257	3.304	0.059	0.1080	0.002	97	1766	27
S308-15	Circular	273	272	3.261	0.048	0.1090	0.001	97	1783	16
L308-29	Pyramidal	270.9	143.8	3.185	0.033	0.1101	0.001	98	1801	15
S308-12	Prismatic	174	159	3.166	0.034	0.1102	0.001	98	1803	16
S308-17	Oblong	205	231.1	3.370	0.068	0.1108	0.002	92	1813	31
S308-34		226.6	199.8	3.159	0.087	0.1108	0.002	98	1813	31
S308-18	Circular	181	105	3.216	0.046	0.1113	0.001	96	1821	20
L308-52	Ovoid	405	378	3.153	0.042	0.1125	0.001	97	1839	15
L308-5		346.3	252.3	2.869	0.047	0.1174	0.002	101	1917	23
L308-49		192	154	2.966	0.049	0.1179	0.001	97	1925	20
S308-32	Circular	213	159	3.012	0.209	0.1229	0.004	92	1999	56
S308-26	Prismatic	99	75	5.453	0.220	0.1417	0.005	48	2248	59

Table 5. LA-ICP-MS data for analyzed zircons from sample 312.

Spot	Morphology	U (ppm)	Th (ppm)	238U/206Pb	±σ	207Pb/206Pb	±σ	Conc. %	207Pb/206Pb (Ma)	±σ
S312-33	Oblong	69.3	57.8	5.970	0.086	0.072	0.002	100	994	48
S312-16	Ovoid	192.8	249	5.291	0.087	0.077	0.001	99	1126	26
L312-90	Oblong	113.5	92.3	4.998	0.112	0.078	0.002	103	1142	43
S312-24		130.7	93.4	5.280	0.081	0.078	0.001	97	1157	30
L312-88	Ovoid	262.3	140.8	4.990	0.060	0.079	0.001	101	1169	20
L312-6	Ovoid	94.8	88.5	5.294	0.064	0.080	0.001	93	1199	30
L312-50		185.8	81.9	4.782	0.082	0.080	0.001	102	1204	34
L312-12	Oblong	356	249	4.610	0.072	0.083	0.001	100	1265	26
L312-53	Circular	152.4	108.4	4.431	0.126	0.083	0.002	103	1276	40
L312-9	Ovoid	98.1	60.9	4.873	0.100	0.084	0.002	93	1295	37
S312-26	Oblong	98.1	77.2	4.651	0.078	0.084	0.002	97	1295	39
L312-77	Oblong	228.1	369	4.435	0.067	0.085	0.001	101	1304	25
L312-17	Oblong	254	224	4.284	0.061	0.085	0.001	103	1314	20
L312-27		52.9	60.1	4.444	0.061	0.085	0.002	99	1320	34
L312-42	Ovoid	143.7	102.4	4.442	0.081	0.085	0.001	99	1322	27
L312-67	Ovoid	103	166.8	4.431	0.080	0.086	0.001	99	1327	32
L312-72	Oblong	82.1	108.7	4.268	0.078	0.086	0.002	102	1327	36
L312-84	Prismatic	85.6	58.2	4.244	0.056	0.086	0.001	103	1327	29
L312-8	Ovoid	315	261	4.464	0.064	0.086	0.001	97	1338	20
L312-87	Oblong	329	539	4.423	0.086	0.086	0.002	98	1338	36
L312-44	Ovoid	338	299	4.266	0.064	0.086	0.001	101	1339	21
L312-85	Prismatic	97	75.9	4.067	0.081	0.086	0.001	106	1343	31
L312-52	Ovoid	197.6	381	4.554	0.137	0.088	0.002	93	1374	44
S312-4	Oblong	22.8	35.9	4.405	0.190	0.088	0.005	96	1374	##
L312-62	Ovoid	404	438	4.535	0.140	0.088	0.001	93	1376	29
S312-15	Circular	351	372	4.264	0.095	0.088	0.001	98	1382	28
L312-40	Oblong	108	70.6	4.214	0.076	0.088	0.001	99	1387	30
L312-38	Circular	105.5	46.8	4.216	0.096	0.089	0.002	98	1393	33
S312-13	Ovoid	197.5	114.9	4.223	0.087	0.089	0.001	98	1400	30
L312-25	Ovoid	25.58	42.6	4.011	0.080	0.090	0.002	101	1419	51
L312-23		65.2	85.5	3.973	0.069	0.091	0.002	101	1436	32
S312-34	Oblong	86.9	114.2	4.202	0.049	0.091	0.002	96	1436	32
L312-18	Oblong	144.8	199.4	4.010	0.076	0.091	0.001	100	1438	25
L312-63	Oblong	401	437	3.956	0.075	0.091	0.001	101	1442	25
L312-33	Oblong	216	262	3.905	0.073	0.091	0.001	102	1445	25
S312-11		251	211.2	3.887	0.069	0.091	0.001	102	1445	29
L312-31	Oblong	196.5	173.1	4.156	0.107	0.091	0.002	96	1447	40
S312-7	Oblong	187.7	234.7	4.011	0.103	0.091	0.002	99	1447	36
L312-70	Ovoid	51.4	57	3.973	0.090	0.091	0.002	100	1449	42
S312-14	Ovoid	134.8	92.5	4.122	0.092	0.091	0.002	97	1449	40
S312-12	Prismatic	264	420	3.928	0.096	0.091	0.002	100	1455	31
L312-49	Ovoid	293.8	319.3	3.891	0.062	0.092	0.001	101	1459	23
L312-51	Circular	123.2	255	3.986	0.079	0.092	0.002	99	1461	33
L312-74		175	108.3	3.912	0.064	0.092	0.001	100	1461	25
L312-83	Ovoid	98.7	167	3.975	0.055	0.092	0.001	99	1461	29
S312-5	Oblong	47.1	45.9	4.156	0.064	0.092	0.002	95	1461	48
L312-79	Ovoid	350	432	3.860	0.064	0.092	0.001	101	1465	25
L312-13	Oblong	302	611	3.994	0.070	0.092	0.001	98	1468	18
L312-16	Oblong	356	269	3.854	0.046	0.092	0.001	101	1470	20
L312-65	Oblong	249.2	223.3	3.954	0.103	0.092	0.002	98	1476	37

Table 5 continued. LA-ICP-MS data for analyzed zircons from sample 312.

Spot	Morphology	U (ppm)	Th (ppm)	238U/206Pb	±σ	207Pb/206Pb	±σ	Conc. %	207Pb/206Pb (Ma)	±σ
L312-26	Oblong	411	326	4.075	0.056	0.092	0.001	96	1477	18
L312-7	Oblong	57.9	80.9	3.849	0.039	0.093	0.001	101	1480	25
L312-10	Ovoid	516.3	645	4.146	0.096	0.093	0.002	94	1486	37
L312-66	Oblong	176.2	99.3	3.650	0.064	0.093	0.001	105	1486	27
L312-75	Oblong	205	351	3.987	0.076	0.093	0.002	97	1486	33
L312-76	Oblong	623	573	4.143	0.079	0.093	0.001	94	1488	29
L312-61	Ovoid	347	328	5.063	0.182	0.093	0.001	78	1488	26
L312-39	Circular	149.4	134.6	3.818	0.061	0.093	0.001	101	1490	26
L312-69	Oblong	262	537	3.864	0.067	0.093	0.001	100	1490	28
L312-54	Oblong	334.3	151	3.781	0.079	0.093	0.001	101	1492	26
L312-21		109.9	90.7	3.781	0.059	0.094	0.001	101	1502	24
L312-37	Prismatic	491	275	3.679	0.077	0.094	0.001	103	1508	24
S312-28	Ovoid	159.4	245.4	3.782	0.054	0.095	0.002	100	1518	30
S312-35	Oblong	101.7	253	3.823	0.039	0.095	0.001	98	1522	26
L312-71	Ovoid	138.8	132.8	3.929	0.074	0.096	0.002	95	1542	29
L312-78	Ovoid	311.4	297.4	3.700	0.053	0.096	0.001	100	1546	19
L312-30	Prismatic	186.5	226.2	3.668	0.058	0.096	0.001	100	1548	22
L312-35	Circular	94.7	189.7	3.704	0.071	0.096	0.001	99	1556	27
L312-56		367	218	3.868	0.120	0.097	0.002	95	1558	45
L312-2	Oblong	154.8	180.6	3.697	0.044	0.097	0.001	99	1559	19
S312-30	Oblong	320.1	333	3.605	0.095	0.097	0.002	101	1569	42
S312-29	Ovoid	258.3	275	3.647	0.063	0.098	0.001	98	1590	27
L312-3	Ovoid	120.7	188	3.551	0.039	0.098	0.001	100	1592	19
L312-14	Ovoid	366	453	3.651	0.047	0.098	0.001	98	1592	17
L312-29	Ovoid	243.4	161.6	3.606	0.056	0.098	0.001	99	1594	23
L312-59	Ovoid	95.9	100.3	3.654	0.064	0.099	0.001	97	1600	26
L312-92	Ovoid	197	137.6	3.337	0.050	0.099	0.001	106	1600	25
S312-3	Ovoid	290.5	109.1	3.449	0.095	0.099	0.002	103	1600	38
L312-73	Circular	327	471	3.583	0.062	0.099	0.001	99	1605	24
S312-27	Ovoid	158	216.1	3.618	0.054	0.099	0.001	98	1609	24
L312-36	Ovoid	197	201.8	3.413	0.075	0.100	0.002	102	1624	30
L312-1	Ovoid	296.5	292.5	3.632	0.051	0.101	0.001	96	1635	18
L312-82	Ovoid	204	190.9	3.455	0.050	0.101	0.001	100	1646	22
S312-22	Circular	209	158.7	3.557	0.086	0.101	0.002	97	1646	37
L312-46	Ovoid	148.5	146.1	3.207	0.056	0.102	0.001	106	1655	26
L312-41	Oblong	458	694	3.542	0.087	0.102	0.002	97	1657	27
L312-15	Ovoid	280	459	3.241	0.047	0.103	0.001	104	1673	20
L312-94	Ovoid	384	309.6	3.158	0.048	0.103	0.001	106	1675	18
S312-31	Ovoid	153.3	117.6	3.376	0.041	0.103	0.001	100	1677	23
S312-2	Circular	135.3	114.8	3.294	0.064	0.103	0.001	102	1682	25
S312-19	Oblong	165.4	157.6	3.205	0.123	0.103	0.003	104	1682	52
S312-20	Ovoid	120.2	106.9	3.339	0.058	0.103	0.002	100	1684	29
L312-58	Oblong	424	411	3.259	0.055	0.104	0.001	102	1691	21
S312-10	Ovoid	193.6	247	3.231	0.075	0.104	0.002	103	1691	34
L312-28	Ovoid	434.7	468.5	3.409	0.070	0.104	0.001	98	1693	23
L312-60	Ovoid	267	233	3.252	0.058	0.104	0.001	102	1700	21
S312-6	Oblong	201.5	187.6	3.313	0.069	0.104	0.002	100	1700	27
L312-48	Ovoid	347	304.6	3.213	0.067	0.105	0.001	102	1706	25
L312-24	Oblong	51.6	46.8	3.393	0.059	0.105	0.002	98	1707	32
L312-47	Ovoid	275	261	3.251	0.067	0.105	0.002	101	1707	26

Table 5 continued. LA-ICP-MS data for analyzed zircons from sample 312.

Spot	Morphology	U (ppm)	Th (ppm)	238U/206Pb	±σ	207Pb/206Pb	±σ	Conc. %	207Pb/206Pb (Ma)	±σ
L312-19	Circular	370	652	3.323	0.051	0.105	0.001	99	1709	19
L312-22		77.3	139	3.223	0.054	0.105	0.002	102	1709	28
L312-89	Ovoid	216	233.7	3.053	0.037	0.105	0.001	107	1711	19
L312-32	Oblong	443	519	3.247	0.056	0.105	0.001	101	1713	21
S312-25	Oblong	411	520	3.269	0.040	0.107	0.001	98	1753	16
L312-20	Ovoid	302	289	3.133	0.050	0.109	0.001	100	1778	22
L312-68	Circular	334	366	3.107	0.052	0.109	0.001	101	1778	17
L312-55	Oblong	351	161.3	3.007	0.082	0.109	0.002	104	1783	33
S312-23	Prismatic	206.8	104	3.164	0.038	0.109	0.001	99	1788	18
L312-80	Prismatic	417	1280	4.026	0.146	0.109	0.001	80	1788	18
L312-91	Prismatic	147.1	106.4	3.007	0.042	0.110	0.001	103	1793	22
L312-57	Pyramidal	257	264.9	3.123	0.059	0.110	0.001	100	1794	22
L312-64	Ovoid	206.6	227	3.060	0.080	0.110	0.002	102	1794	30
S312-21	Oblong	193	235	3.107	0.035	0.110	0.001	100	1796	18
L312-86	Prismatic	379.7	634	3.420	0.048	0.110	0.001	92	1798	18
L312-45	Pyramidal	113.2	106.9	3.036	0.049	0.110	0.001	102	1799	20
L312-11	Pyramidal	471	567	3.073	0.051	0.110	0.001	101	1801	23
S312-8	Oblong	137.4	158.8	3.114	0.051	0.110	0.001	100	1801	23
L312-43	Ovoid	153	103.4	3.030	0.072	0.111	0.002	102	1808	31
S312-18	Prismatic	232	235	3.144	0.046	0.111	0.001	98	1809	20
L312-93	Oblong	460	368	3.007	0.044	0.111	0.001	102	1813	16
L312-4	Oblong	207.9	250.5	3.087	0.032	0.111	0.001	100	1813	16
L312-81	Prismatic	598	1291	3.833	0.075	0.111	0.001	82	1816	16
L312-5	Circular	159.8	129.2	2.804	0.031	0.122	0.001	99	1983	15
L312-34	Oblong	89.9	82.7	1.961	0.046	0.184	0.003	99	2690	25

II. Geochronology - principles and analytical instruments.

The advent of Geochronology can be traced back to when the relationship of Lead and Uranium was first discussed in association with measurement of geological time (Arthur Holmes 1911). Further investigations into U-decay and U-Pb chemical geochronology contributed to creating one of the most common and valuable isotopic dating methods today (Barrell 1917; Holmes & Lawson 1927).

Lead occurs as four naturally stable isotopes: ^{204}Pb, ^{206}Pb, ^{207}Pb and ^{208}Pb. The last three of these have a radiogenic component that is formed by decay of ^{238}U, ^{235}U and ^{232}Th respectively (Schoene 2014). The popularity of the U-PB system is in part due to the high amount of minerals that are rich in Uranium. These minerals are in turn also often resistant to physical and chemical weathering and occur in a wide array of different rocks (Schoene 2014). Common minerals for U-Pb dating include allanite, apatite, baddeleyite, monazite, perovskite, rutile, titanite, zircon and xenotime. With zircon being the most commonly used (Corfu et al. 2003).

Three different decay chains exist within the U-Th-Pb system:

- $^{238}U \rightarrow ^{206}Pb$ with a chronometer based on the measurement of $^{206}Pb/^{238}U$,
- $^{235}U \rightarrow ^{207}Pb$ with a chronometer based on the measurement of $^{207}Pb/^{235}U$
- $^{232}Th \rightarrow ^{208}Pb$ with a chronometer based on the measurement of $^{208}Pb/^{232}U$

They have a half-life of 4.47 Ga, 0.70 Ga and 14.01 Ga respectively (Gehrels 2014). Furthermore an age can be calculated using $^{206}Pb/^{207}Pb$ when it's assumed that most crustal rocks have a constant $^{238}U/^{235}U$ ratio of 137.82 (Hiess et al. 2012):

Equation 1:

$$\frac{(206Pb/238U)}{(207Pb/235U)} = \frac{(206Pb/207Pb)}{(238U/235U)} = \frac{(206Pb/207Pb)}{137.82}$$

The main isotopes measured for Zircon are $^{206}Pb/^{238}U$, $^{206}Pb/^{207}Pb$ and $^{206}Pb/^{204}Pb$. Zircon has generally low Th concentrations so $^{208}Pb/^{232}Th$ is seldom used. Furthermore the Pb/Th system could be detached from the Pb/U system (Gehrels 2014). The $^{207}Pb/^{235}U$ ratio is not used since a more reliable calculation can be gained using equation 1 (Gehrels 2014). $^{206}Pb/^{204}Pb$ is measured in order to correct the $^{206}Pb/^{238}U$ and $^{206}Pb/^{207}Pb$ ratios for Pb that was included when the zircon crystallised. This is commonly referred to as correcting for initial Pb (Gehrels 2014).

Using a mass spectrometer to measure the ratios of $^{206}Pb/^{207}Pb$ and $^{206}Pb/^{204}Pb$ is fairly straightforward as we're only dealing with Pb. While measuring $^{206}Pb/^{238}U$ a problem crops up because Pb and U fractionate at different rates during an analysis (Gehrels 2014). Two different techniques are used to correct for this fractionation: Isotope dilution that involves the dissolution of the crystal and yields isotope ratios with a high precision at around 0.1% (See Gehrels 2014 for in-depth explanation) and standard-sample bracketing that is used herein. Standard-sample bracketing determines the true amount of $^{206}Pb/^{238}U$ using a correction factor between measured $^{206}Pb/^{238}U$ and known $^{206}Pb/^{238}U$. This is done by continuously measuring the $^{206}Pb/^{238}U$ ratios of zircons (Called standards) with known $^{206}Pb/^{238}U$ ratios and comparing these to the ratios obtained while measuring. The measurements doesn't require dissolution of zircons and yield precision and accuracy at about 1% (Gehrels 2014).

The most frequent way of visualising the two chronometers is through the use of a concordia diagram (Wetherill 1956). This diagram is designed to display the decay systems of $^{238}U \rightarrow ^{206}Pb$ and $^{235}U \rightarrow ^{207}Pb$ as well as the critical ratios of $^{206}Pb^*/^{238}U$, $^{207}Pb^*/^{235}U$ and $^{206}Pb^*/^{207}Pb^*$, with asterisks denoting correction for initial Pb (Gehrels 2014). When the three ratios gives similar ages interpreting the age is fairly simple, the analyses overlap the Concordia and they are referred to as being concordant (Gehrels 2014). A discordant analysis occurs when the U-Pb system has been disturbed and the three ratios yields different dates, and in turn plot away from the concordia (Gehrels 2014).

Disturbances of the U-Pb system can occur through inheritance, where for instance several grains of differing ages or zircon grains containing multiple age domains are measured (Gehrels 2014). Furthermore discordance can occur due to Pb loss, where some form of disturbance after crystallisation causes the more mobile Pb to disappear in greater extent compared to U (Gehrels 2014). The more discordant an analysis becomes the greater the effect of inheritance and Pb loss. For Pb loss this takes the form of the calculated date becoming less accurate. For $^{206}Pb^*/^{207}Pb^*$ the effect of discordance on the accuracy is smaller which makes it the most reliable for zircons over 1.2 Ga old. They are however always underestimates of the true age (Gehrels 2014). $^{206}Pb^*/^{238}U$ dates are more reliable when it comes to inheritance but they are always overestimates of the true age (Gehrels 2014).

When handling data important decisions needs to be made regarding which chronometers to use (I.e $^{206}Pb^*/^{238}U$ for concordant analyses of grains older than 1.2 Ga) and whether to exclude discordant analyses (Gehrels 2014). Usually discordant analyses are not taken into consideration when detecting specific age groups, however they can be used to determine proportions of age groups within a sample (Gehrels 2014).

Dating of detrital zircons is especially useful when dealing with sedimentary rocks that lack fossils for biostratigraphy, a sedimentary unit cannot be older

than the youngest zircon grain present (Gehrels 2014). Pb loss and the naturally occurring uncertainty of an analysis can result in interpreted ages that are younger than the actual one. In order to produce a reliable age the youngest group of ages are often weighted to produce a mean age, or the age distributions of the analyses are summed to create a peak age (Gehrels 2014).

A scanning electron microscope (SEM) is used to determine optimal analytical spots for laser ablation inductively coupled plasma mass spectrometer (LA-ICP-MS) analysis. This method utilizes back scattered electron imaging (BSE) and/or cathodoluminescence imaging (CL) (Schoene 2014).

A SEM fires a high-energy electron beam at a sample causing many secondary features to appear (Egerton 2005). With the microscope in BSE-mode heavy elements (e.g. Uranium) appear brighter than lighter elements and thus areas with greater concentrations of heavy minerals can be determined and examined (Egerton 2005).

Cathodoluminescence induces a sample using a focused beam of electrons causing it to emit light. This light is collected by an optical instrument wherein the components wavelengths are separated in a monochromator elucidating sample element composition (Nasdala et al. 2003).

A LA-ICP-MS ablates a sample with a laser beam. The ablated particles are subsequently carried by various gases into a mass spectrometer that analyses their chemical composition (Schoene 2014). The LA-ICP-MS is made up of two parts: The laser ablation unit with the sample holder and the mass spectrometer containing the plasma. The lasers usually uses short wavelengths (266 nm or less) and are of either solid-state or gas-source type (Schoene 2014).

Determining the origin of sediments through geochronology is done using the ages of detrital zircons and comparing them with known ages for suites of rocks that could be the possible proto-source (Gehrels 2014). Ideally the zircons collected should represent an unbiased representation of the sample, in reality this is very hard to accomplish (Gehrels 2014). A number of strategies exist to produce an unbiased age distribution: The zircons should be picked in a way that does not bias towards any group based on size, morphology or chemistry whilst picking them in a random fashion (Sircombe & Stern 2002; Gehrels 2014), the analytical methods should enable the study of various sized zircons (Gehrels 2014), grains should not be skipped completely and BSE/CL imaging should be used to determine optimal analysis spots as well as detecting signs of changes in $^{206}Pb/^{238}U$ during analyses that could indicate complexities (Gehrels 2014), data should be displayed with a focus on the most reliable characteristics like precision, lower discordance and belonging to clusters (Gehrels 2014), sufficient data should be obtained to hold statistical significance in order to distinguish between various age components depending on the study in question (Gehrels 2014).

Tidigare skrifter i serien ”Examensarbeten i Geologi vid Lunds universitet”:

494. Larsson, Måns, 2016: TEM investigation on Challapampa aquifer, Oruro Bolivia. (45 hp)
495. Nylén, Fredrik, 2017: Utvärdering av borrhålskartering avseende kalksten för industriella ändamål, File Hajdarbrottet, Slite, Gotland. (45 hp)
496. Mårdh, Joakim, 2017: A geophysical survey (TEM; ERT) of the Punata alluvial fan, Bolivia. (45 hp)
497. Skoglund, Wiktor, 2017: Provenansstudie av detriala zirkoner från ett guldförande alluvium vid Ravlunda skjutfält, Skåne. (15 hp)
498. Bergcrantz, Jacob, 2017: Ett fönster till Kattegatts förflutna genom analys av bottenlevande foraminiferer. (15 hp)
499. O'Hare, Paschal, 2017: Multiradionuclide evidence for an extreme solar proton event around 2610 BP. (45 hp)
500. Goodship, Alastair, 2017: Dynamics of a retreating ice sheet: A LiDAR study in Värmland, SW Sweden. (45 hp)
501. Lindvall, Alma, 2017: Hur snabbt påverkas och nollställs luminiscenssignaler under naturliga ljusförhållanden? (15 hp)
502. Sköld, Carl, 2017: Analys av stabila isotoper med beräkning av blandningsförhållande i ett grundvattenmagasin i Älvkarleby-Skutskär. (15 hp)
503. Sällström, Oskar, 2017: Tolkning av geofysiska mätningar i hammarborrhål på södra Gotland. (15 hp)
504. Ahrenstedt, Viktor, 2017: Depositional history of the Neoproterozoic Visingsö Group, south-central Sweden. (15 hp)
505. Schou, Dagmar Juul, 2017: Geometry and faulting history of the Long Spur fault zone, Castle Hill Basin, New Zealand. (15 hp)
506. Andersson, Setina, 2017: Skalbärande marina organismer och petrografi av tidigcampanska sediment i Kristianstadsbassängen – implikationer på paleomiljö. (15 hp)
507. Kempengren, Henrik, 2017: Föroreningsspridning från kustnära deponi: Applicering av Landsim 2.5 för modellering av lakvattentransport till Östersjön. (15 hp)
508. Ekborg, Charlotte, 2017: En studie på samband mellan jordmekaniska egenskaper och hydrodynamiska processer när erosion påverkar släntstabiliteten vid ökad nederbörd. (15 hp)
509. Silvén, Björn, 2017: LiDARstudie av glaciala landformer sydväst om Söderåsen, Skåne, Sverige. (15 hp)
510. Rönning, Lydia, 2017: Ceratopsida dinosauriers migrationsmönster under krittiden baserat på paleobiogeografi och fylogeni. (15 hp)
511. Engleson, Kristina, 2017: Miljökonsekvensbeskrivning Revinge brunnsfält. (15 hp)
512. Ingered, Mimmi, 2017: U-Pb datering av zirkon från migmatitisk gnejs i Delsjöområdet, Idefjordenterrängen. (15 hp)
513. Kervall, Hanna, 2017: EGS - framtidens geotermiska system. (15 hp)
514. Walheim, Karin, 2017: Kvartsmineralogins betydelse för en lyckad luminiscensdatering. (15 hp)
515. Aldenius, Erik, 2017: Lunds Geotermisystem, en utvärdering av 30 års drift. (15 hp)
516. Aulin, Linda, 2017: Constraining the duration of eruptions of the Rangitoto volcano, New Zealand, using paleomagnetism. (15 hp)
517. Hydén, Christina Engberg, 2017: Drumlinerna i Löberöd - Spår efter flera isrörelseriktningar i mellersta Skåne. (15 hp)
518. Svantesson, Fredrik, 2017: Metodik för kartläggning och klassificering av erosion och släntstabilitet i vattendrag. (45 hp)
519. Stjern, Rebecka, 2017: Hur påverkas luminiscenssignaler från kvarts under laboratorieförhållanden? (15 hp)
520. Karlstedt, Filippa, 2017: P-T estimation of the metamorphism of gabbro to garnet amphibolite at Herrestad, Eastern Segment of the Sveconorwegian orogen. (45 hp)
521. Önnervik, Oscar, 2017: Ooider som naturliga arkiv för förändringar i havens geokemi och jordens klimat. (15 hp)
522. Nilsson, Hanna, 2017: Kartläggning av sand och naturgrus med hjälp av resistivitetsmätning på Själland, Danmark. (15 hp)
523. Christensson, Lisa, 2017: Geofysisk undersökning av grundvattenskydd för planerad reservvattentäkt i Mjölkalånga, Hässleholms kommun. (15 hp)
524. Stamsnijder, Joaen, 2017: New geochronological constraints on the Klipriviersberg Group: defining a new Neoarchean large igneous province on the Kaapvaal Craton, South Africa. (45 hp)
525. Becker Jensen, Amanda, 2017: Den eocena Furformationen i Danmark: exceptionella bevaringstillstånd har bidragit till att djurs mjukdelar fossiliserats.(15 hp)
526. Radomski, Jan, 2018: Carbonate sedimentology and carbon isotope stratigraphy of the Tallbacken-1 core, early Wenlock Slite Group, Gotland, Sweden. (45 hp)
527. Pettersson, Johan, 2018: Ultrastructure

and biomolecular composition of sea turtle epidermal remains from the Campanian (Upper Cretaceous) North Sulphur River of Texas. (45 hp)

528. Jansson, Robin, 2018: Multidisciplinary perspective on a natural attenuation zone in a PCE contaminated aquifer. (45 hp)
529. Larsson, Alfred, 2018: Rb-Sr sphalerite data and implications for the source and timing of Pb-Zn deposits at the Caledonian margin in Sweden. (45 hp)
530. Balija, Fisnik, 2018: Stratigraphy and pyrite geochemistry of the Lower–Upper Ordovician in the Lerhamn and Fågelsång -3 drill cores, Scania, Sweden. (45 hp)
531. Höglund, Nikolas, 2018: Groundwater chemistry evaluation and a GIS-based approach for determining groundwater potential in Mörbylånga, Sweden. (45 hp)
532. Haag, Vendela, 2018: Studie av mikrostrukturer i karbonatslagkäglor från nedslagsstrukturen Charlevoix, Kanada. (15 hp)
533. Hebrard, Benoit, 2018: Antropocen – vad, när och hur? (15 hp)
534. Jancsak, Nathalie, 2018: Åtgärder mot kusterosion i Skåne, samt en fallstudie av erosionsskydden i Löderup, Ystad kommun. (15 hp)
535. Zachén, Gabriel, 2018: Mesosideriter – redogörelse av bildningsprocesser samt SEM-analys av Vaca Muertameteoriten. (15 hp)
536. Fägersten, Andreas, 2018: Lateral variability in the quantification of calcareous nannofossils in the Upper Triassic, Austria. (15 hp)
537. Hjertman, Anna, 2018: Förutsättningar för djupinfiltration av ytvatten från Ivösjön till Kristianstadbassängen. (15 hp)
538. Lagerstam, Clarence, 2018: Varför svalde svanödlor (Reptilia, Plesiosauria) stenar? (15 hp)
539. Pilser, Hannes, 2018: Mg/Ca i bottenlevande foraminiferer, särskilt med avseende på temperaturer nära 0°C. (15 hp)
540. Christiansen, Emma, 2018: Mikroplast på och i havsbotten - Utbredningen av mikroplaster i marina bottensediment och dess påverkan på marina miljöer. (15 hp)
541. Staahlnacke, Simon, 2018: En sammanställning av norra Skånes prekambriska berggrund. (15 hp)
542. Martell, Josefin, 2018: Shock metamorphic features in zircon grains from the Mien impact structure - clues to conditions during impact. (45 hp)
543. Chitindingu, Tawonga, 2018: Petrological characterization of the Cambrian sandstone reservoirs in the Baltic Basin, Sweden. (45 hp)
544. Chonewicz, Julia, 2018: Dimensionerande vattenförbrukning av grundvatten samt alternativa vattenkvaliteter. (15 hp)
545. Adeen, Lina, 2018: Hur lämpliga är de geofysiska metoderna resistivitet och IP för kartläggning av PFOS? (15 hp)
546. Nilsson Brunlid, Anette, 2018: Impact of southern Baltic sea-level changes on landscape development in the Verkeån River valley at Haväng, southern Sweden, during the early and mid Holocene. (45 hp)
547. Perälä, Jesper, 2018: Dynamic Recrystallization in the Sveconorwegian Frontal Wedge, Småland, southern Sweden. (45 hp)
548. Artursson, Christopher, 2018: Stratigraphy, sedimentology and geophysical assessment of the early Silurian Halla and Klinteberg formations, Altajme core, Gotland, Sweden. (45 hp)
549. Kempengren, Henrik, 2018: Att välja den mest hållbara efterbehandlingsmetoden vid sanering: Applicering av beslutsstödsverktyget SAMLA. (45 hp)
550. Andreasson, Dagnija, 2018: Assessment of using liquidity index for the approximation of undrained shear strength of clay tills in Scania. (45 hp)
551. Ahrenstedt, Viktor, 2018: The Neoproterozoic Visingsö Group of southern Sweden: Lithology, sequence stratigraphy and provenance of the Middle Formation. (45 hp)

LUNDS UNIVERSITET

Geologiska institutionen
Lunds universitet
Sölvegatan 12, 223 62 Lund